Surface Acid Properties of Nb_2O_5-P_2O_5-SiO_2 Gel-Derived Catalysts

Gabriella Garbarino[1], Giovanni Pampararo[2], Elisabetta Finocchio[1], Guido Busca[1*], Antonella Gervasini[3], Sebastiano Campisi[3], Brigida Silvestri[4], Claudio Imparato[4], Antonio Aronne[4*]

[1] Dipartimento di Ingegneria Civile, Chimica e Ambientale, Università di Genova, Via Opera Pia 15, I-16145 Genova, Italy.
[2] Dipartimento di Chimica e Chimica Industriale, Università di Genova, Via Dodecaneso 31, I-16146 Genova, Italy
[3] Dipartimento di Chimica, Università degli Studi di Milano, Via Camillo Golgi 19, I-20133 Milano, Italy.
[4] Dipartimento di Ingegneria Chimica, dei Materiali e della Produzione Industriale, Università di Napoli Federico II, P.le Tecchio, 80, I-80125, Napoli, Italy.

*Corresponding authors: anaronne@unina.it; guido.busca@unige.it

Abstract

Amorphous catalytic materials belonging to the Nb_2O_5-P_2O_5-SiO_2 system were prepared through an original sustainable sol-gel procedure, and characterized by surface area, porosity and acidity measurements. Their acid properties have been investigated by FTIR spectroscopy of adsorbed pyridine, ammonia titration and TPR, as well as by titration with 2-phenylethylamine from organic solution. They present Lewis acidity attributed to niobium surface cationic centers, and Brønsted acidity sufficiently strong to protonate pyridine. The total acidity depends on the niobium content. The conversion of ethanol was investigated by vapor phase Temperature Programmed Reaction, steady-state catalytic experiments and static In Situ FTIR experiments. The samples are active in converting ethanol to ethylene with 100 % selectivity at low conversion (523-573 K), but also produce acetaldehyde by dehydrogenation at higher temperature and conversion. They show an unusually poor activity for the production of diethylether also at low ethanol conversion. Ethoxy groups act as reaction surface intermediates.

Keywords: acid solids; sol-gel; ethanol dehydration; niobia; phosphoric anhydride.

1. Introduction

Solid acid catalysts play a very relevant role in industrial chemistry [1]. Very strong acidic materials, such as protonic zeolites [2], are mostly needed to activate very weak σ-type bases such as paraffins as well as quite electron deficient π-type bases such as e.g. ethylene for alkylation reactions. Indeed, these materials play a key role in the refinery and petrochemistry fields [3]. Weaker protonic solid acids [4], such as e.g. the so called "solid phosphoric acid" catalyst (SPA) [5,6], can also be applied for less demanding reactions, e.g. for protonation of more electron-rich olefins to produce oligomerization or aromatic alkylations. Moderately strong protonic solid acids, and Lewis acids as well, may be even more performant in activating stronger n-type bases, such as oxygenates, and for this reason they may play an even more important role in the renewable industrial chemistry based on biomass conversions. For this application, acid water tolerant catalytic materials are also needed, since they are generally employed in aqueous solution or exposed to humidity. In these processes, niobium and phosphorus-based catalysts are widely used owing to tunable distribution of both Brønsted and Lewis acidic sites combined with high stability towards hydrolysis given by Nb–O–P bonds [7]. In particular, the niobium-phosphorus-silicon mixed oxide systems emerged as an environmentally friendly and performant system for biomass conversion. Previous studies showed that, while silica is characterized by low surface protonic acidity, P_2O_5 provides significantly stronger Brønsted acidity [8] while niobia provides both Brønsted and Lewis acidity [9,10,11,12].

A hydrolytic sol–gel procedure was developed by some of the authors to synthesize Nb_2O_5–P_2O_5–SiO_2 (Nb-P-Si) materials [13,14] which were proved to be effective catalysts in dehydration of fructose, hydrolysis of inulin and esterification of oleic acid with polyalcohols for biolubricant production [15,16]. The proper incorporation of a niobium phosphate phase into a silica matrix allows a fine dispersion of acid sites over a large surface area, even with relatively low amounts of Nb and P, with highly stable anchorage of phosphorous into the matrix.

In this scenario, following the principles of sustainable chemistry, a new chloride-free sol–gel procedure has been recently performed using ammonium niobium oxalate and phosphoric acid as both precursors and acid catalysts, water as solvent and no additional mineral acid catalysts. The obtained ternary oxides showed promising acid-type catalytic activity [17]. The aim of the present work is a more extensive assessment of the acidic

properties of this family of catalytic materials in terms of strength, distribution and accessibility of acid sites. Moreover, the reactivity of the samples towards ethanol was studied by spectroscopic analyses and ethanol temperature programmed surface reaction. The product distribution observed allows to confirm the potentiality of the samples as selective acidic catalysts.

2. Experimental

2.1 Synthesis procedure

Niobium–phosphorus–silicon mixed oxide materials were prepared by a hydrolytic sol–gel synthesis following our previously reported procedure [17]. Tetraethoxysilane, $Si(OC_2H_5)_4$, TEOS, (98%, Sigma- Aldrich), phosphoric acid (85 wt% solution, AppliChem), ammonium niobium oxalate hydrate, $NH_4[NbO(C_2O_4)_2(H_2O)_2]\cdot nH_2O$, ANbO (kindly supplied by Companhia Brasileira de Metallurgia e Mineração, CBMM), were used as precursors.

Sample with two different molar compositions were synthesized: $2.5Nb_2O_5\cdot 2.5P_2O_5\cdot 95SiO_2$ and $5Nb_2O_5\cdot 2.5P_2O_5\cdot 92.5SiO_2$, indicated in the following as 2.5Nb2.5PSi and 5Nb2.5PSi, respectively. Briefly, a proper amount of ANbO was added to a mixture of TEOS and deionized water, followed by the addition of H_3PO_4, then the system was stirred at room temperature until gelation occurred. The gels were aged, dried in air at temperature up to 383 K, then the xerogels were annealed in air at 773 K for 1 h at the heating rate of 10 K min^{-1}.

2.2 Morphological characterization

N_2 adsorption and desorption isotherms were collected at liquid nitrogen temperature (77 K) on an automatic analyser of surface area (Sorptomatic 1990 version instrument from Thermo Scientific Carlo Erba). Before the experiments, fresh and treated samples at 573 K and 773 K (maintained for 1 h) were outgassed at 423 K for 16 h (ca., 0.15 g, 80-200 mesh). Surface area values were computed from 3-parameters BET equation in the range $0.05<p/p_0<0.4$. Microporous volume and micropore size were calculated using Saito and Foiley (S-F) model in the interval $0<p/p_0<0.35$ using the nitrogen on zeolite potential-function [18]. Conventional BJH model was used for mesoporosity determination. The adsorbed volume, expressed in cm^3 (STP) $\cdot g^{-1}$, was converted into pore volume, $cm^3\cdot g^{-1}$, considering the density of N_2 in the normal liquid state $\rho = 0.8081$ g $cm\cdot g^{-1}$); molecular area of N_2 was taken as 16.2 $Å^2$.

2.3 Surface acidity studies

Qualitative characterization of the surface acid sites at the vapor/solid interface was realized by a FT-IR study of adsorbed pyridine. Samples have been activated in vacuum (10^{-3} torr) at 753 K and 823 K. Pyridine adsorption (2 torr vapor) was performed at room temperature and following outgassing at increasing temperatures. Spectra of the pure powder disks were recorded at each adsorption/desorption step, using a Thermonicolet Nexus instrument (100 scans, OMNIC software).

Gas-solid titrations were performed by NH_3 probe adsorption in flowing dynamic experiments in a home-made adsorption line equipped with mass flow controllers for gas flow regulation, an electrical vertical oven for temperature control and linked to a FT-IR spectrophotometer (Bio-Rad with DTGS detector). A quartz reactor packed with pellets of the sample (*ca*. 0.1 g, particles in the range of 80-200 mesh dried at 373 K overnight) was placed inside the oven. The samples were pre-treated at 393 K under flowing nitrogen for 30 min. prior to the measurements in order to desorb impurities and remove physically adsorbed water. Then, a NH_3/N_2 mixture, with NH_3 concentration of *ca*. 500 ppm flowed at 4 NL h^{-1} through the reactor maintained at 393 K. The gas flow at the outlet of the reactor entered in a gas cell (path length 2.4 m multiple reflection gas cell) in the beam of the FT-IR spectrophotometer where it was measured online (monitoring NH_3 line at 966 cm^{-1}, N-H asymmetric stretching, wagging mode). The number of acid sites (in μequiv·g^{-1}) was determined by quantitatively evaluating the adsorbed NH_3.

Thermo-desorption analysis of ammonia (NH_3-TPD) was carried out on NH_3-saturated samples by operating in the line above described. Approximately 60 mg of sample (80-200 mesh particle size) was pre-treated in the quartz tubular sample-holder at 393 K for 30 min under N_2 flowing at 50 ml·min^{-1}. Ammonia saturation was achieved by flowing 1% NH_3/N_2 at 50 ml·min^{-1} for ca. 50-60 min at 298 K. The adsorbed NH_3 was monitored following continuously the NH_3 line at 966 cm^{-1} as a function of time. After attainment of saturation, at first, an isothermal step at 423 K was performed under N_2 flowing (50 ml·min^{-1}) to remove the excess of adsorbed ammonia from the surface (physisorbed) until attainment of a stable signal. Then, temperature was raised at 10 K·min^{-1} up to 1073 K and TPD spectrum was recorded. A typical scheme of NH_3-TPD experiment is illustrated in Fig. S1.

Acid site titrations in solid-liquid phase using 2-phenylethylamine (PEA) as probe were carried out in a recirculation chromatographic line (HPLC), consisting of a pump (Waters mod. 515) and a monochromatic UV detector (Waters mod. 2487, working at fixed λ = 254 nm), coupled to a personal computer for the collection, storage, and processing of the data.

The samples (ca. 0.03 g, crushed and sieved as 80-200 mesh particles) were placed between two sand pillows in a stainless steel sample-holder (length 12 cm, i.d. 2 mm) mounted in place of the chromatographic column and surrounded by a glass jacket thermostated by circulating water (303.0±0.1K). Before each experiment, the sample underwent a thermal pre-treatment (423 K in 8 mL min^{-1} air flux for 16 h) and then it was conditioned in the same solvent employed as eluent (cyclohexane).

A first adsorption was performed by repeatedly injecting successive dosed amounts of PEA solution (50 µL, ca. 0.10 M) into the chromatographic line. A step-chromatogram was obtained, where each step represents the achieving of adsorption equilibrium. First adsorption was considered concluded, when at least three successive injections gave identical step height in the chromatogram, indicating that saturation was attained and no sites were available for PEA adsorption. After the collection of the first adsorption isotherm on fresh sample (I° run), pure solvent flowed through the saturated sample overnight (ca. 16 h), thus permitting desorption of the probe molecules from weakly interacting sites. Then, a second adsorption of PEA on the same sample was repeated (II° run) to titrate weak acid sites and evaluate strong acid sites by difference.

2.4. Studies of the surface reactivity towards ethanol

2.4.1 Ethanol Temperature Programmed Surface reaction (EtOH-TPSR)

Ethanol surface programmed surface reaction were conducted in a continuous fixed bed reactor in non-oxidative and oxidative environments. In each experiment, 43 mg of the sample were mixed with 127 mg of calcined sand (60-70 mesh Sigma-Aldrich, stabilized at 1073 K for 5 h). The temperature was increased (373-773 K) with a ramping rate of 5 K/min, and, at the end, the maximum temperature of 773 K was kept constant for 15 minutes.

For non-oxidative experiments, either 1 mol% or 2.5 mol% of ethanol in pure nitrogen was fed at the flow rate of 170 NmL/min. For the experiments in oxidative conditions the feed was 1 mol% EtOH/6% O_2/93% N_2, i.e. with an oxygen content sufficient to obtain full ethanol combustion. In all cases, the GHSV is around 220000 h^{-1}. The product analysis was realized by continuous online FT-IR analysis (Nicolet 380 FT-IR spectrometer) equipped with a home-made gas cell.

2.4.2 FT-IR studies of ethanol adsorption and reactivity

Ethanol adsorption was performed at room temperature after activation in vacuum of the sample. In a first step, two spectra were recorded: catalyst in the presence of ethanol vapor and after short outgassing at room temperature applied in order to have only some residual

ethanol vapor in gas phase (< 1 torr). After this step, thermal evolution of both adsorbed and gas phase species was studied in static conditions and in the range 423-723 K, by recording spectra of the surface and of the gas phase species.

2.5 Ethanol conversion catalytic experiments.

Steady state experiments were carried out in oxidative environment in the same conditions used in Oxidative Ethanol TPSR. Catalytic material was loaded with a higher amount of sand (43 mg catalyst powder in 300 mg of sand) in order to avoid non-isothermal behavior in the catalytic bed. Temperature is increased step by step from 373 to 773 K, with a temperature interval of 50 K and a dwelling time of 30 minutes.

To evaluate the effect of contact time, experiments were realized in non oxidative conditions (1 and 3 mol% ethanol in nitrogen), at relatively low temperatures, 673 K and 573 K. Catalysts were diluted in sand (43 mg catalyst powder in 300 mg of sand). Three different space velocities were tested, obtained by varying the total flow rate, 100, 150 and 200 mL/min, corresponding to GHSV around 130000 h^{-1}, 190000 h^{-1} and 260000 h^{-1}.

3. Results and discussion

3.1 Morphology characterization.

It has been already shown [17] that the adopted sol-gel synthesis produced *water-tolerant* Nb-P-Si solid acids featuring a tunable distribution of Nb- and P-species in the silicate framework and the firm anchorage of P in the matrix. The choice of ammonium niobium oxalate as precursor allowed the control of the Nb coordination number influencing the hydrolysis of Nb oligomers in the sol and in turn the distribution of Nb polyhedra in the gels. As derived from previously reported solid state NMR, FT-IR and Raman investigation [17] an amorphous silicate network including $NbOPO_4$ nanocrystals, already showing a high degree of cross-linking, was obtained in dried gels. During the thermal treatment at 773 K further self/cross-condensation reactions occurred between Nb-, P- and Si-units ultimately producing an amorphous structure composed of Nb–O–Si and/or Nb–O–Nb and P–O–Nb and/or P–O–P bridges. The calcination at high temperature did not negatively influence the morphological properties of the samples. Really, both dried and 573 K-calcined gels had surface area values only a little higher (10%-20%) than those calcined at 773 K (Table 1).

The detailed results on the morphological characterization of the calcined samples (773 K), 2.5Nb2.5PSi and 5Nb2.5PSi, based on the collected N_2 adsorption/desorption isotherms, are reported In Table 1. Both samples have N_2-adsorption/desorption isotherms typical of microporous solids (Type I, IUPAC classification), showing asymptotic trends typical of

Table 1. Morphological properties of the ternary oxidic samples

Sample	Total Surface Area[a] $m^2\ g^{-1}$	*Mesoporosity* [b]		*Microporosity* [c]	
		Pore $Size_{av}$ nm	Pore Volume $cm^3\ g^{-1}$	Pore $Size_{av}$ nm	Pore volume $cm^3\ g^{-1}$
2.5Nb2.5PSi	407 C_{BET}: 164 N_{av}:1.5	5.3	0.02	1.3	0.16
5Nb2.5PSi	365 $C_{BET:}$ 156 N_{av}: 2.6	3.4	0.06	1.6	0.17

[a] Obtained from the 3-parameters BET fit, in the $0.05 < p/p^0 < 0.4$ interval

[b] Most representative pore population computed from B.J.H. model on the desorption isotherm branch in the $0.3 < p/p^0 < 0.95$ interval with standard universal isotherm (Harkins-Jura) (ASTM Standards Designation: D 4641-87)

[c] Calculated from p/p^0 0 to 0.35 with potential function: nitrogen on zeolite at 77 K, from literature [18].

Langmuirian curves and absence of clear hysteresis (Fig. 1, a1 and 1, b1). The 2.5Nb2.5PSi sample shows a more pronounced Langmuirian curve than 5Nb2.5PSi and, accordingly, the computed microporous size is smaller for 2.5Nb2.5PSi (1.3 nm) than for 5Nb2.5PSi (1.6 nm). Micropore distributions in the 0-4 nm range (pore radius) have been detailed for two samples in Fig. 1, a3 and 1, b3. The presence of mesopores cannot be completely ruled out, actually BJH equation indicates poor mesoporous volume, as expected, associated with small mesopore size, of 5.3 nm for 2.5Nb2.5PSi and 3.4 nm for 5Nb2.5PSi. Then, from the morphologic analysis, it can be inferred that in both samples microporosity predominates over the mesoporosity. As concerns this latter, structural effect deriving from the presence of Nb oxide component, which acts as bridge between Si and P units, might be responsible for higher mesoporosity in 5Nb2.5PSi than 2.5Nb2.5PSi.

The values of surface area are similar to those previously reported for other Nb-P-Si samples [13,14]. The lower surface area value of 5Nb2.5PSi (365 $m^2 \cdot g^{-1}$) with respect to 2.5Nb2.5PSi (407 $m^2 \cdot g^{-1}$) is likely due to the lower amount of SiO_2, decreased from 84.8 wt.% to 76.7 wt%.

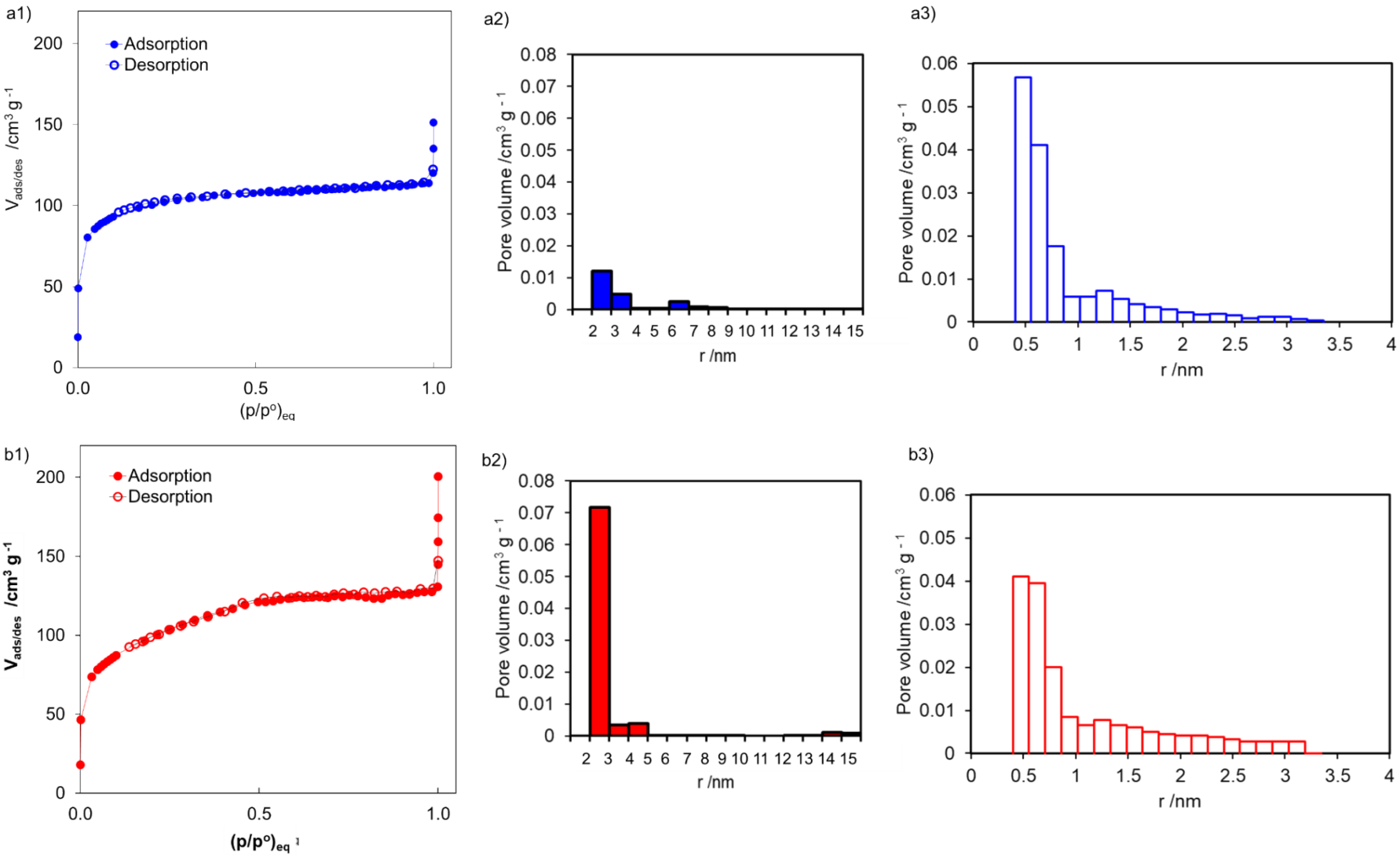

Figure 1. Morphologic characterization of 2.5Nb2.5PSi sample (a) and 5Nb2.5PSi (b) samples treated at 773 K. N_2 adsorption and desorption isotherms at 77 K (a1 and b1), mesopore size distribution determined by BJH model equation from the desorption branch of the N_2-isotherms (a2 and b2), and micropore size distribution determined by Saito and Foiley model equation (a3 and b3) [18].

3.2 Surface structure and acidity characterization

Qualitative analyses of the surface structure and surface acidity of the samples were realized using FT-IR spectroscopy of pure powder pressed disks at the vacuum/vapour/solid interface. The FT-IR spectrum of the 2.5Nb2.5PSi sample after outgassing at 763 K (Fig. 2, a) shows in the OH stretching region two main components, a broad and ill-defined absorption with two apparent maxima around 3700 and 3665 cm^{-1}, together with a sharper component centered near 3740-3720 cm^{-1}. The latter is associated to the presence of isolated silanol Si-OH species, typically located in that range [19], while the former component can be assigned to a combination of P-OH and Nb-OH groups [20,21]. After outgassing at 823 K, i.e. at temperature higher than the calcination temperature of these samples, a noticeable dehydration of the surface occurs, reducing the absorption in the whole region 3700-3200 cm^{-1}, in large part due to H-bonded OH groups (Fig. 2, b). Only silanols are still detected evident (free and residual H-bonded silanols), while the other bands are only observable as shoulders. As expected, adsorbing water over the same surface (Fig. 2, c) results in a reconstitution of hydroxyl groups other than free silanols characterized by a broad absorption centered near 3650 cm^{-1}, consistent with the attribution to P-OH species, and a very broad absorption centered around 3300 cm^{-1}, due to H-bonded water and hydroxy groups.

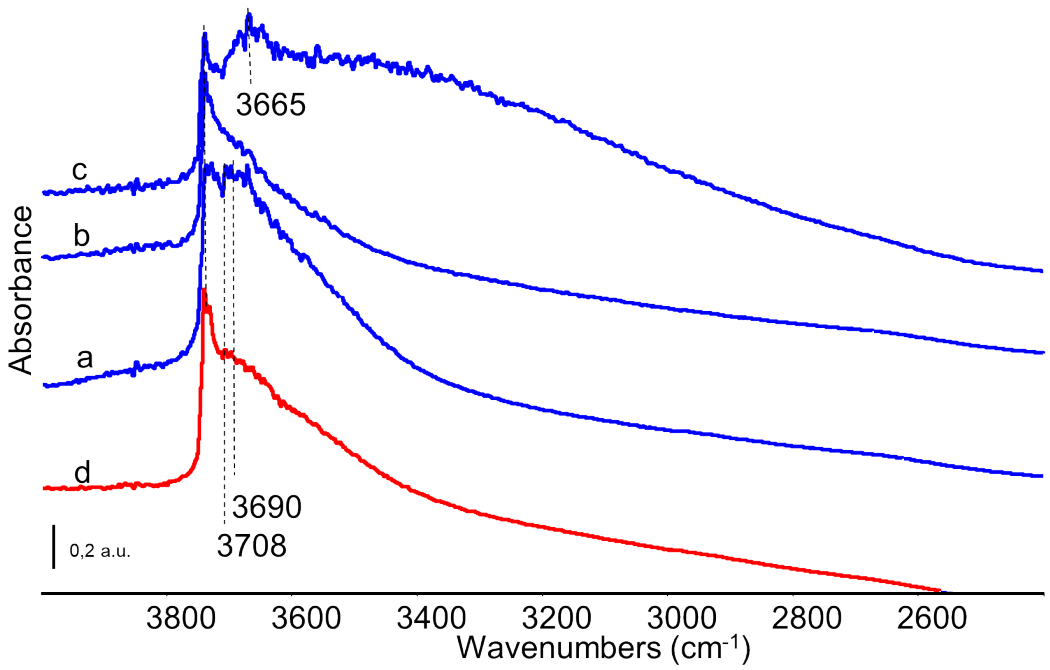

Figure 2. FT-IR spectra of samples in the OH stretching region. 2.5Nb2.5PSi sample (blue) after outgassing at 763 K (a), at 823 K (b) and after subsequent contact with water vapor and short outgassing (c). Spectrum of 5Nb2.5PSi sample (red) after outgassing at 763 K (d).

The spectrum of the 5Nb2.5PSi sample after outgassing at 763 K (Fig. 2, d) is very similar to that of the 2.5Nb2.5Si sample outgassed at 823 K, suggesting that the addition of more niobium oxide results in a stronger interaction or to condensation with the OH groups that are hydrogen bonded in the case of the lower Nb content sample.

The nature of the surface acidity has been investigated by FT-IR spectroscopy using pyridine as an adsorbed probe. Over the 2.5NbPSi sample (Fig. 3), pyridine adsorption and outgassing at room temperature evidences the presence of both molecularly adsorbed species and protonated species. Molecular species are characterized by the detection of the 8a vibrational modes at 1595 and 1609 cm^{-1}, and 19b vibrational mode at 1448 cm^{-1}, with a shoulder at lower frequencies. The shift of these bands to higher wavenumbers with respect to those reported for the free molecule (1583 and 1436 cm^{-1}, respectively) is an evidence of the interaction of these species with electron-withdrawing centers [22]. While the couple of bands at 1595 cm^{-1} and around 1440 cm^{-1} can be likely indicative of a medium-strong hydrogen bonding (as it may occur with the weakly acidic silanol groups), the bands at 1609 and 1448 cm^{-1} are certainly associated to the interaction with quite strong Lewis acid sites. The latter adsorbed species are still detectable up to 623 K and a very small shift towards higher frequencies at decreasing coverage is within the resolution of the instrument. Taking into account that tetravalent silicon (such as in silica and silicates [23]) and pentavalent phosphorous as well [24] are not able to provide Lewis acidity, these species would confirm the Lewis acidity of pentavalent niobium, as also found on the surface of pure niobic acid [25] as well as of niobia-silica [26].

The absorptions at 1638 and 1545 cm^{-1} are instead certainly due to pyridinium ion (8a and 19a modes [22]), thus they provide evidence of the presence of Brønsted acid sites. Brønsted acidic sites able to protonate pyridine are absent on pure silicas, while are present on P_2O_5-SiO_2 [27], Nb_2O_5-SiO_2 [26], niobic acid [25] and niobium phosphate [21], and are consequently to be attributed to Nb-OH and/or P-OH groups.

Thus, these data confirm the presence of Si-OH, Nb-OH and P-OH groups, free and H-bonded, and the presence of both Brønsted and Lewis acidity in the samples, as previously reported for differently prepared Nb-P-Si samples [14-16].

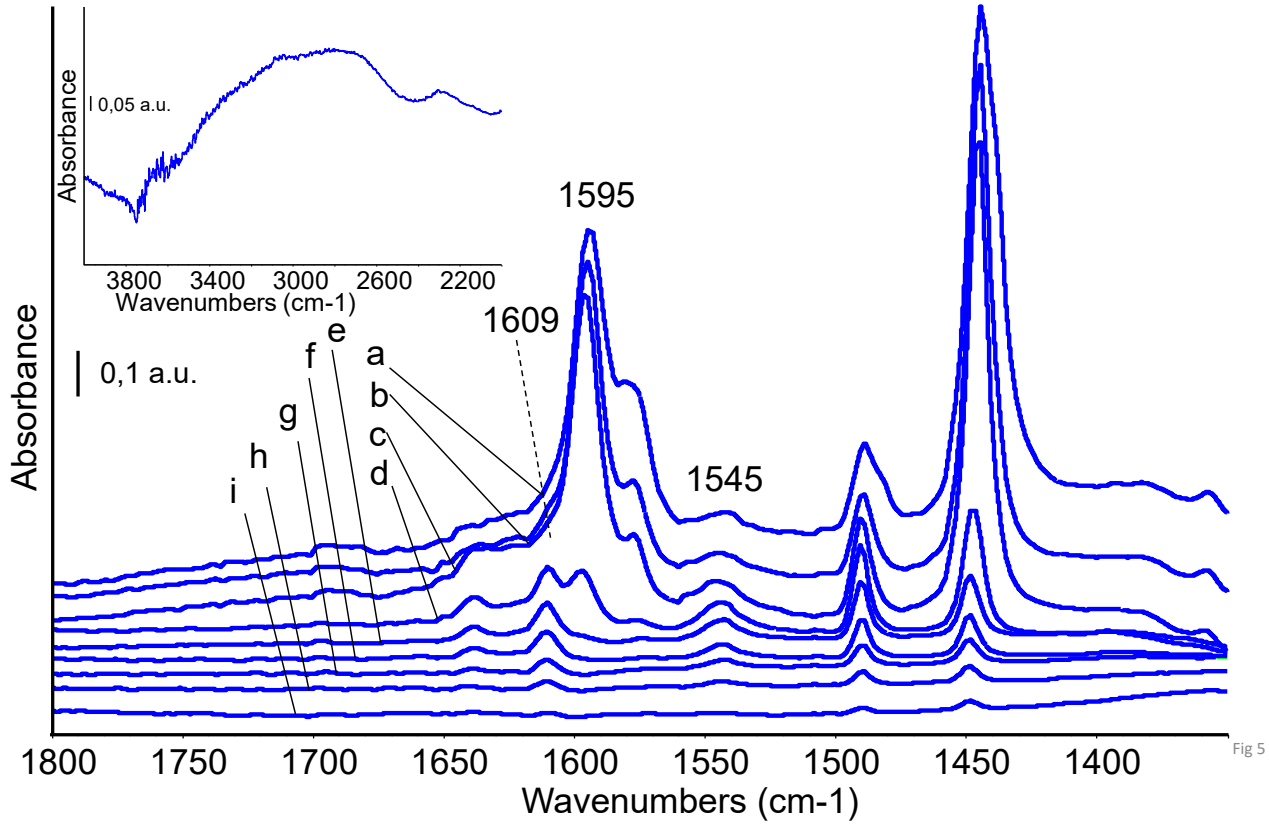

Figure 3. FT-IR subtraction spectra of adsorbed surface species arising from pyridine adsorption at room temperature over 2.5Nb2.5PSi sample (a) and after outgassing at room temperature (b), prolonged outgassing at room temperature (c and inset: OH stretching region), outgassing at 423 K (d), 473 K (e), 523 K (f), 573 K (g), 623 K (h), 673 K (i). The activated surface spectrum has been subtracted.

Also over the 5Nb2.5PSi sample, pyridine adsorption and outgassing at room temperature (Fig. 4) provide evidence of the presence of both exposed Lewis sites and Brønsted sites, whose main diagnostic bands are located at 1608 cm^{-1} (shoulder, 8a vibrational mode of Lewis-bonded molecular pyridine) and 1545 cm^{-1} (19a mode of pyridinium ion), respectively.

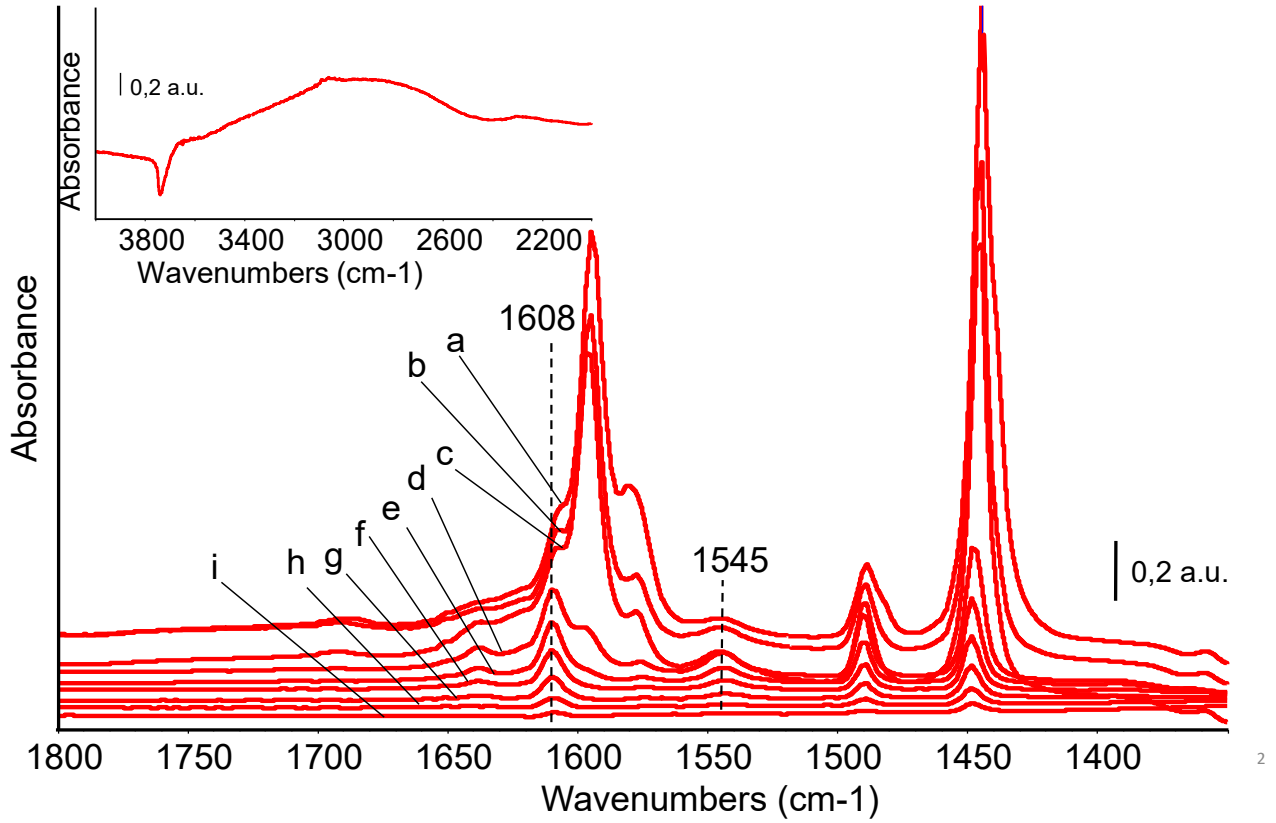

Figure 4. FT-IR subtraction spectra of adsorbed surface species arising from pyridine adsorption at room temperature over 5Nb2.5PSi sample (a) and after outgassing at room temperature (b), prolonged outgassing at room temperature (c and inset, OH stretching region), outgassing at 423 K (d), 473 K (e), 523 K (f), 573 K (g), 623 K (h), 673 K (i). The activated surface spectrum has been subtracted.

The comparison of Fig. 4 with spectra reported in Fig. 3 shows that the shoulder above 1600 cm^{-1} assigned to pyridine coordinated over Lewis sites is already more evident in the spectrum of sample 5Nb2.5PSi recorded after outgassing at room temperature, in agreement with the highest Nb load over this catalyst. Indeed, this band becomes sharper and clearly centered at 1608 cm^{-1} after outgassing at increasing temperature. For both catalysts, OH bands described above appear as negative features in the subtraction spectra (insets in Figs. 3 and 4), consistent with the interaction of different families of hydroxyls with pyridine molecules (H-bonding and protonation).

In another set of experiments, 5Nb2.5PSi catalyst has been pretreated with water vapor directly in the IR cell before pyridine adsorption. After water vapor adsorption a broad band is detected in the range 3650-2800 cm^{-1} due to OH stretching mode of molecularly adsorbed water interacting with the surface hydroxyl groups through H-bonds. The corresponding deformation mode is detected as sharp and strong band at 1632 cm^{-1} (Fig. S2). A short outgassing leads to the decrease in intensity of these features whereas the band assigned

to isolated silanol is already partially restored at 3740 cm^{-1} pointing out the partial desorption of molecular water. Interestingly, no evidence of protonated water is observed, in agreement with the lower basicity of water with respect to pyridine, that is instead partly protonated. Over the “wet” surface, pyridine adsorption has been performed at room temperature, followed by desorption at increasing temperature (Fig. 5 for sample 5Nb2.5PSi). The spectrum recorded after pyridine adsorption and a short outgassing at room temperature shows the main bands previously discussed for molecular and protonated pyridine adsorbed over the dry surface, i.e. the peaks at 1596, 1546, 1490 and 1445 cm^{-1}. A broad and ill-defined adsorption centered at 1622 cm^{-1} is due to molecularly adsorbed water overlapped with the component near 1640 cm^{-1} due to pyridinium ions. A shoulder at 1608 cm^{-1} is still detectable, pointing out that pyridine coordinates over exposed Lewis sites even after pretreatment in water, in agreement with previous results reported on pyridine adsorption from aqueous phase over Nb-P-Si ternary oxide [16] and on hydrated Nb_2O_5 heterogeneous catalysts [28], as well as on other acidic oxides as alumina and silica-alumina [29].

This effect is not surprising considering that indeed pyridine is a stronger base than water, thus displacing water molecules from Lewis sites. Features of pyridine over Lewis sites become more evident following prolonged outgassing and, finally, the spectrum recorded at 423 K is completely consistent with the corresponding spectrum recorded over the dry catalyst surface. On the other side, at 423 K the B/L ratio (ratio of number of Brønsted and Lewis sites), evaluated as [Intensity of the band at 1546 cm^{-1}/Intensity of the band at 1608 cm^{-1}], increases on the wet surface, and this could be due to more abundant Brønsted sites, due to the dissociative adsorption of water.

Once again, the high frequency region of the subtraction spectra shows negative and complex band due to silanol species that interact with pyridine. Moreover, by subtracting the spectrum of the wet surface (i.e. the highly hydroxylated surface) from the spectrum after pyridine adsorption we have the evidence of the complexity of the OH groups, with evidence of several components at 3730, 3700 and 3640 cm^{-1} (Fig. S3), which, according to previous literature [19,20,21], could be due to Si-OH, Nb-OH and P-OH groups, respectively.

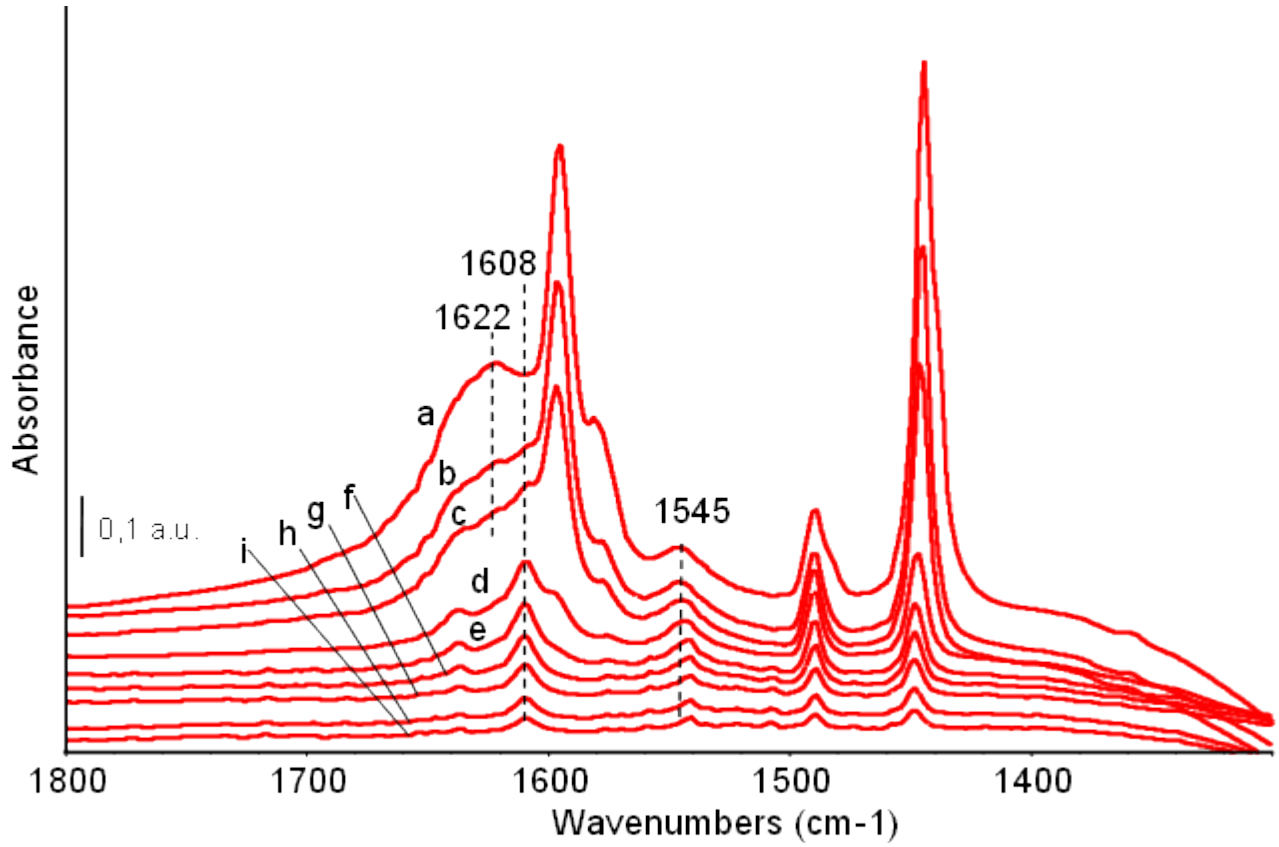

Figure 5. FT IR subtraction spectra of adsorbed surface species arising from pyridine adsorption at room temperature over wet 5Nb2.5PSi sample (a) and after outgassing at room temperature (b), prolonged outgassing at room temperature (c), outgassing 423 K (d), 473 K (e), 523 K (f), 573 K (g), 623 K (h), 673 K (i). The activated surface spectrum has been subtracted.

Samples acidity was studied quantitatively carrying out acid-base titrations by using ammonia as a basic probe in the gas phase, and 2-phenylethylamine (PEA) in the liquid phase. The two probes are both highly basic, but they have different kinetic diameters. NH_3 is a very small molecule with a kinetic diameter of 2.6 Å, that allows entering into almost all the micropores of 2.5Nb2.5PSi and 5Nb2.5PSi and thus probing the acid sites present at both internal and external surfaces. Conversely, the larger PEA molecule, with dimensions of approximately 7 Å, may not have access to the exposed acid sites on the inner surface of micropores. Therefore, the comparison of the titration results with NH_3 and PEA probes could provide valuable information on the accessibility of acid sites in the two samples. Ammonia titration was carried out under gas-solid phase, while PEA titration under liquid-solid phase, by using an apolar and aprotic solvent, cyclohexane, to have an inert environment.

The adsorbed amounts of NH_3 and PEA calculated from the collected adsorption isotherms are reported in Table 2, expressed as acid site number (μmol g^{-1}) and acid site density (μmol m^{-2}).

Table 2. Surface acid sites of the Nb-P-Si samples measured with NH_3 (for gas-solid phase titration) and PEA (for liquid-solid phase titration) probes.

Sample	NH_3 Probe (gas-solid)		PEA Probe (liquid-solid)	
	Acid site number μmol g^{-1}	*Acid site density* μmol m^{-2}	*Acid site number* μmol g^{-1}	*Acid site density* μmol m^{-2}
2.5Nb2.5PSi	463.35 ± 22.11	1.14 ± 0.12	234 ± 8 (91%) [a]	0.58 ± 0.08
5Nb2.5PSi	536.96 ± 6.01	1.48 ± 0.15	457± 15 (37%) [a]	1.25 ± 0.17

[a] Strong acid sites, in percent.

Regarding gas-solid phase NH_3 titration, 5Nb2.5PSi adsorbs a slightly larger amount (537 μmol g^{-1}) of basic probe than 2.5Nb2.5PSi (463 μmol g^{-1}). This difference may be expected because it reflects the different composition of the two materials; indeed, the higher the Nb content (5Nb2.5PSi), the more abundant the acid sites are, as expected in relation to the Lewis and Brønsted acidity provided by niobium centres. It is interesting to note that 5Nb2.5PSi showed more acid character than 2.5Nb2.5PSi even if it possesses lower surface area (Table 1), thus showing also a higher acid site density. In fact, the surface of the silica component does not provide Lewis acidity nor Brønsted acidity sufficiently strong to protonate ammonia [23].

Liquid–solid PEA adsorption isotherms are reported in Fig. 6. The obtained curves show asymptotic profiles, which are well fitted by Langmuir model. The total number of sites reported in Table 2 (234 μmol g^{-1} and 457 μmol g^{-1} for 2.5Nb2.5PSi and 5Nb2.5PSi, respectively) was computed from the first isotherm collected at 303.0 K (assuming a 1:1 stoichiometry for the PEA adsorption on the acid site). After solvent flowing and cleaning, a second adsorption was realized; from the difference between the number of PEA adsorbed moles in the first and second runs, the so called “irreversibly” adsorbed amount of PEA was computed with the possibility to evaluate strong acid sites of the samples.

In the case of 2.5Nb2.5PSi, the acidity probed by PEA (234 μmol g^{-1}) is almost 50% of the total acidity measured using ammonia (463 μmol g^{-1}), while only a slight decrease is observed for 5Nb2.5PSi, comparing the NH_3 (537 μmol g^{-1}) and PEA (457 μmol g^{-1}) titrations. These outcomes agree with morphological analysis (Table 1), showing that the

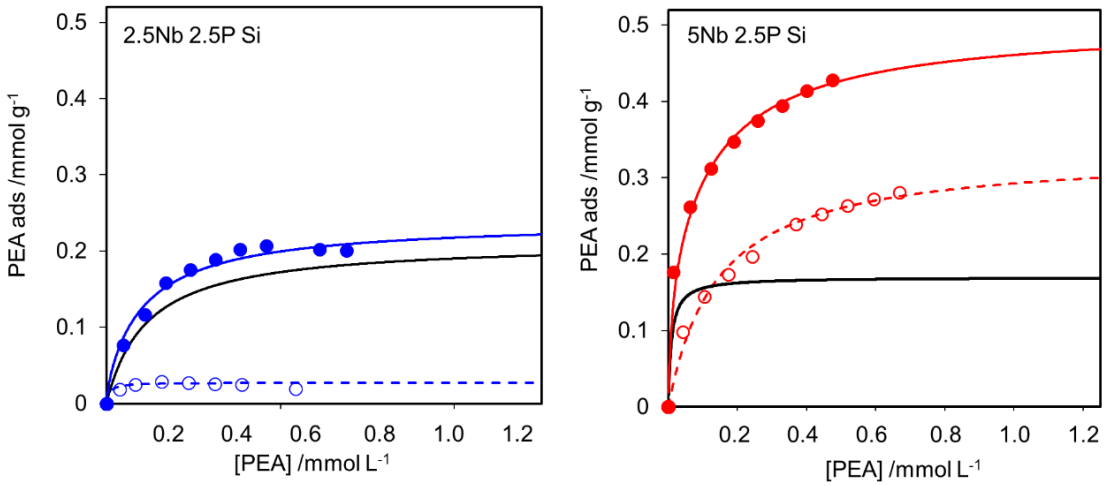

Figure 6. Adsorption isotherms of PEA probes at 303 K on 2.5Nb2.5PSi (left panel) and 5Nb2.5PSi (right panel) samples evaluated in cyclohexane, for determining the *intrinsic* acidity. Full markers and empty markers represent the I° and the II° run adsorptions, respectively. Black lines represent the calculated Langmuir curves of PEA adsorptions on strong acid sites; (blue and red) dotted lines represent the calculated Langmuir curves of the II° runs; blue and red lines represent the adsorption trends of the I° runs, obtained as sum of the dotted and the black lines.

accessibility of acid sites is lower in 2.5Nb2.5PSi, which possesses smaller micropores than 5Nb2.5PSi.

Concerning the number of strong acid sites, almost the totality (91%, corresponding to ca. 213 μmol g^{-1}) of acid sites probed by PEA are strong sites in 2.5Nb2.5PSi, whereas strong sites account for only 37% of acid sites titrated in 5Nb2.5PSi (169 μmol g^{-1}). Likely, the higher Nb-concentration in 5Nb2.5PSi results mainly in a higher number of weaker Brønsted/Lewis sites at the surface.

The presence of a larger amount of strong sites in 2.5Nb2.5PSi than in 5Nb2.5PSi was confirmed by NH_3-TPD experiments (Fig. 7), which revealed that NH_3 desorbed from 2.5Nb2.5PSi and 5Nb2.5PSi surfaces with comparable strength (T_{max} was observed at *ca.* 618 K in any case), but in different amount (430 μmol g^{-1} and 367 μmol g^{-1} for 2.5Nb2.5PSi and 5Nb2.5PSi, respectively).

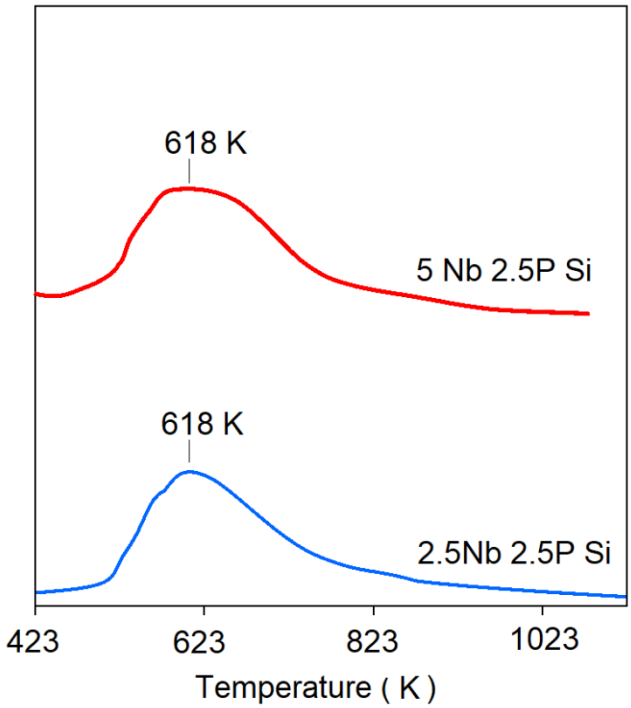

Figure 7. NH_3-TPD profiles as a function of temperature of 2.5Nb2.5PSi (blue) and 5Nb2.5PSi (red) calcined (773 K), collected as described in Experimental section. Both 2.5Nb2.5PSi and 5Nb2.5PSi samples showed the same value of T_{max} (*ca*. 618 K). The amount of desorbed ammonia was 430.5 μmol g^{-1} for 2.5Nb2.5PSi and 367.2 μmol g^{-1} for 5Nb2.5PSi.

3.3 Catalytic conversion of ethanol in Temperature Programmed Surface Reaction conditions.

In Fig. 8 the results of ethanol TPSR with 1 % ethanol feed are reported. In both cases, the light-off temperature for ethanol conversion is found at ~ 550 K, with ethylene as the only

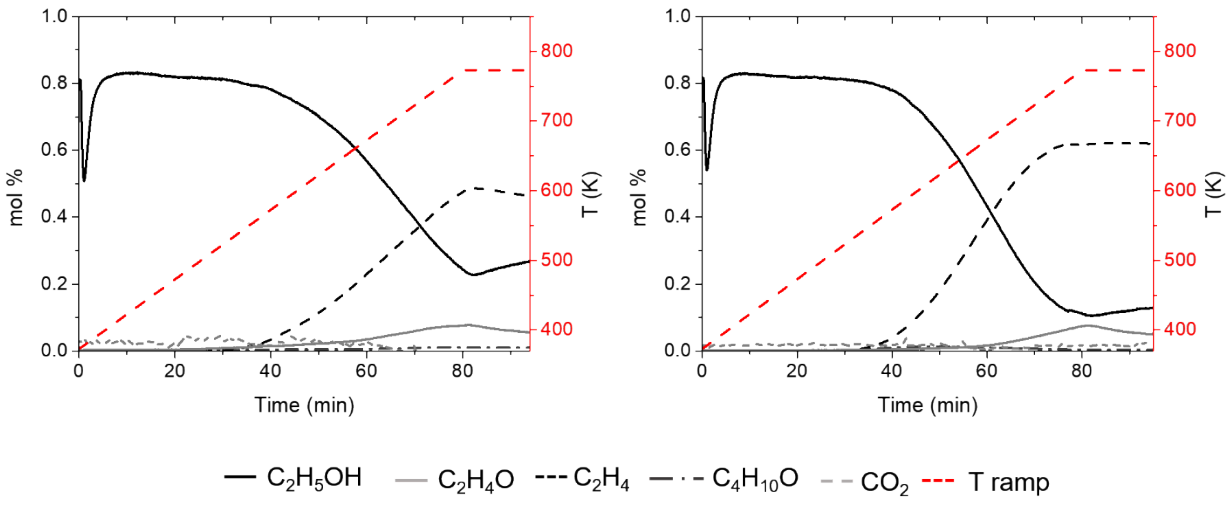

Figure 8. Ethanol TPSR experiments with 1% Ethanol feed: 2.5Nb2.5PSi left, 5Nb2.5PSi right.

product, followed by acetaldehyde production with light-off at ~ 650 K. Thus, the following reactions are observed to occur:

$CH_3CH_2OH \rightarrow H_2C=CH_2 + H_2O$ (1)

$CH_3CH_2OH \rightarrow CH_3CHO + H_2$ (2)

i.e. monomolecular dehydration and dehydrogenation, respectively. With both catalysts, in the last part of the experiment the temperature increase was stopped at 773 K and a dwelling step at constant temperature was realized. At 773 K ethanol conversion is 76% and 87 % over 2.5Nb2.5PSi and 5Nb2.5PSi, respectively, suggesting that additional niobium results in increased reaction rate, likely due to increased acid density. This agrees with the above data. In fact, the dehydration reactions do not need strong acidity, thus the more abundant acidity of 5Nb2.5PSi, despite being constituted by relatively weak sites (see above), allows higher catalytic activity than 2.5Nb2.5PSi. Upon the dwelling step, ethanol conversion and both ethylene and acetaldehyde yields were decreasing with time over 2.5Nb2.5PSi catalyst, suggesting that active sites for both reactions undergo partial deactivation. In contrast, over the 5Nb2.5PSi catalyst only acetaldehyde yield decreases with time in the dwelling time, ethylene yields being nearly constant. In any case, no other products, including di-ethyl-ether and ethyl-acetate, were observed in these experiments. Thus, ethylene selectivity is essentially 100% at low conversion in the 550-650 K range over both catalysts. Ethylene selectivity decreases to 87 %, with 13 % selectivity to acetaldehyde, at 773 K over 2.5Nb2.5PSi, while over 2.5Nb5PSi the selectivities to ethylene and acetaldehyde at 773 K are 89% and 11%, respectively.

The same experiment has been repeated using a higher ethanol partial pressure, with 2.5 % ethanol / nitrogen feed, whose results are reported in Fig. 9.

The curve observed on 2.5Nb2.5PSi is similar to the previous one although the conversion of ethanol is lower at each temperature and product selectivity ratio is slightly shifted towards acetaldehyde (77% ethylene; 23 % acetaldehyde at 773 K). In contrast, the increase in ethanol feed molar fraction produces a more important variation on the product distribution over the 5Nb2.5PSi catalyst; in this case, acetaldehyde starts to be produced already at 500 K, achieving a maximum at 773 K with a selectivity as high as 0.33 mol.% (ethylene selectivity 67%).

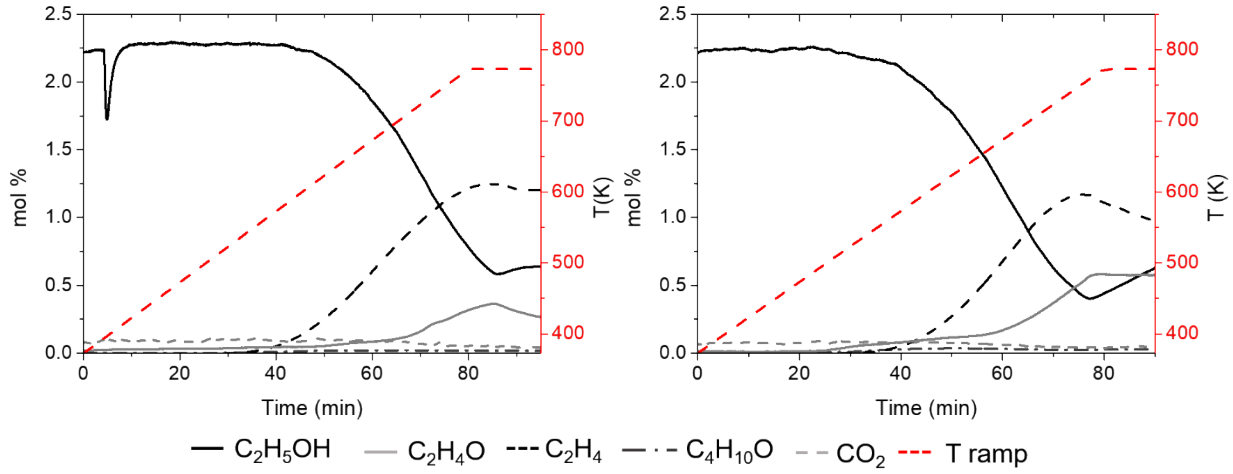

Figure 9. Ethanol TPSR experiments with 2.5 % Ethanol feed: 2.5Nb2.5PSi left, 5Nb2.5PSi right.

This suggests that the additional niobium sites in 5Nb2.5PSi catalyst are more active in dehydrogenation reaction (2) than those present in 2.5Nb2.5PSi catalyst. Again, diethyl ether and ethyl-acetate are not observed in significant quantities.

Taken into consideration the slight deactivation phenomenon observed in the dwelling step in previous experiments (which may have several different origins), and the production of acetaldehyde (that can occur via pure dehydrogenation but also by oxidative dehydrogenation), experiments have been carried out in oxidizing conditions too. The oxygen feed content chosen is in principle sufficient to allow full ethanol combustion. Experiments in oxidative conditions were carried out at the same ethanol molar fraction chosen for the non-oxidative ethanol TPSR experiments in order to evaluate the effect of oxygen in the same fluido-dynamic conditions (Fig. 10). Oxygen introduction is not affecting the light-off temperatures for ethanol conversion, ethylene and acetaldehyde production (with a very small increase in acetaldehyde selectivity) but it only shows a prominent effect in the increase of the acetaldehyde content at temperatures above 600 K, and stabilizing its yield in the dwelling step.

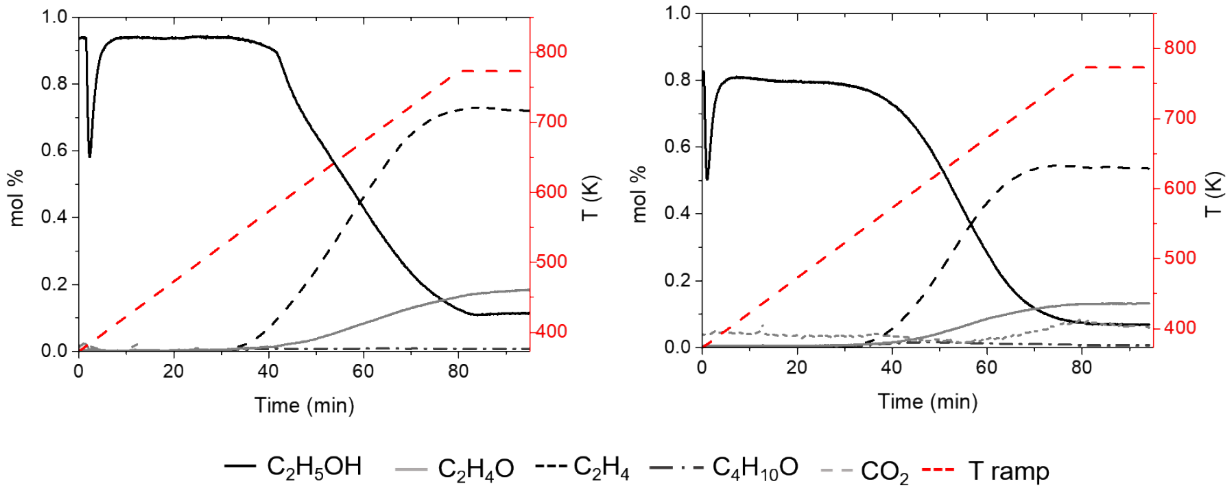

Figure 10. Oxidative Ethanol TPSR experiments, with 1% EtOH/ 6% O_2/ 93% N_2: 2.5Nb2.5PSi left, 5Nb2.5PSi right.

For the higher Nb loading, also CO_2 appears at high temperature among reaction products, certainly coming from ethanol total oxidation. These data suggest that the presence of oxygen does not affect the dehydration and the (pure) dehydrogenation reactions to ethylene and acetaldehyde, while stopping the deactivation effect in the dwelling step. This effect can be due to limiting niobium reduction to lower oxidation states and (at least for 5Nb2.5PSi catalyst) burning carbonaceous material deposited on the surface.

3.4 Catalytic conversion of ethanol in Steady State conditions

In Fig. 11, the results for steady state experiments are reported. They have been realized in the presence of oxygen, taking into consideration the limited effect of oxygen on product selectivity and the positive effect in limiting deactivation. The results are in good agreement with those obtained in transient conditions, showing that ethylene is main product for the whole T range. 5Nb2.5PSi is more active than 2.5Nb2.5PSi at 623 and 673 K in ethylene production and, for this catalyst, no temperature effect is observed above 723 K, suggesting possible diffusion limitation or a change in the catalyst structure. The best ethylene yields are obtained at 773 K over the 5Nb2.5PSi catalyst, at 88 mol% ethanol conversion, 83 mol% selectivity to ethylene, and 11 % selectivity to acetaldehyde and 6 % to CO_2. Over the 2.5Nb2.5PSi catalyst conversion is definitely lower as well as ethylene selectivity. Also in these conditions, the production of diethylether and ethylacetate is near zero.

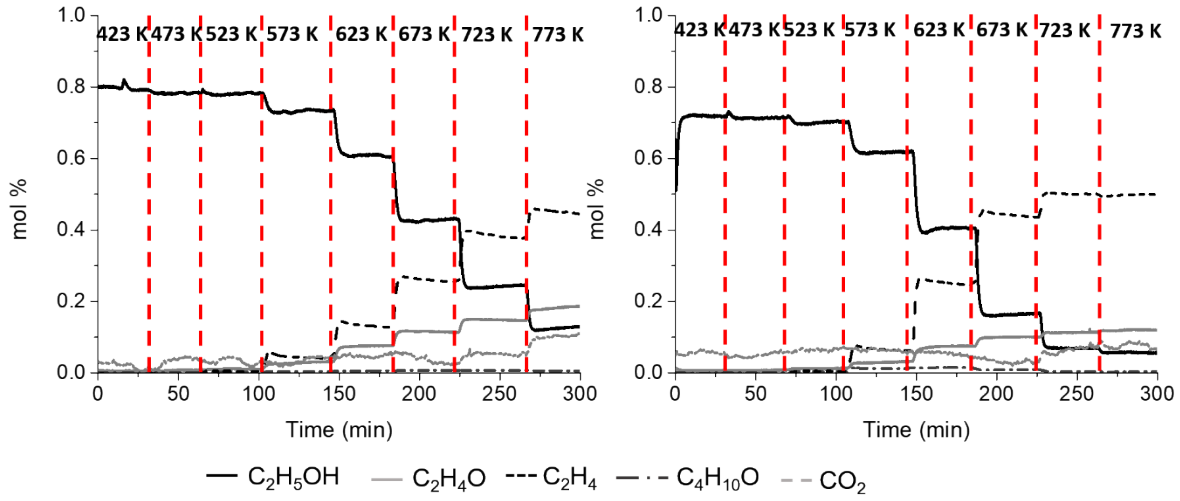

Figure 11. Results of steady state experiments: 2.5Nb2.5PSi left, 5Nb2.5PSi right.

3.5 Study of the effect of contact time on catalytic conversion

The effect of contact time has been evaluated, by choosing two different ethanol feed molar fractions, and working at low ethanol conversion. In Figs. 12, 13 and 14, the obtained concentration profiles as a function of time and total flow rate are reported. These data confirm that 2.5Nb2.5PSi is less active than 5Nb2.5PSi, even though both show an almost total selectivity towards ethylene in such low conversion conditions. However, small amounts of dethylether are observed at low flow rate, but decreases almost to zero at higher flow rate. This suggests that diethylether is a secondary product, while ethylene is the primary product. Thus, diethylether should not form as usual by dehydration of ethanol,

$$2\ CH_3CH_2OH \rightleftharpoons (CH_3CH_2)_2O + H_2O \qquad (3)$$

occurring [30,31] at lower temperature and conversion than dehydration to ethylene (reaction (1), but from addition of ethanol to ethylene

$$CH_3CH_2OH + H_2C{=}CH_2 \rightleftharpoons (CH_3CH_2)_2O \qquad (4)$$

As expected, at lower flow rates, i.e. higher contact times, the conversion of ethanol is markedly higher than at higher flow rates. On the other hand, the effect of contact time is more pronounced in the case of the more active catalyst (5Nb2.5PSi) and with the lower ethanol concentration. Indeed, ethanol conversion is higher at lower ethanol feed concentration, suggesting that a self-inhibition occurs, leading to a negative reaction order of ethanol in the production of ethylene. The effect of contact time is far less evident at lower reaction temperatures, where conversion is very low (Fig. 14).

Catalysts deactivation is more remarkable at the lower Nb loading, possibly due to the higher density of very strong acid sites, and at lower flow rate.

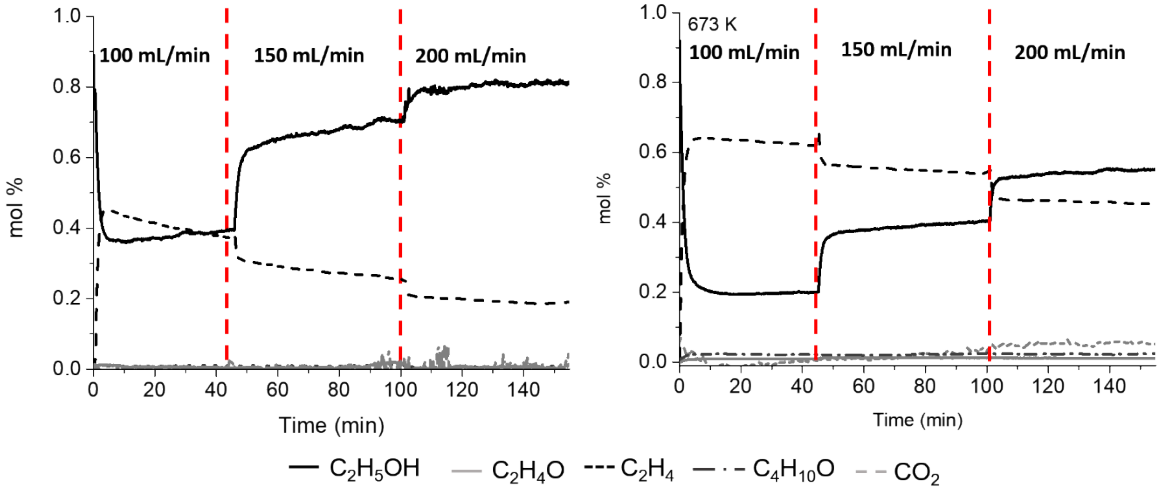

Figure 12. 2.5Nb2.5PSi left, 5Nb2.5PSi right, 1% EtOH at 673 K.

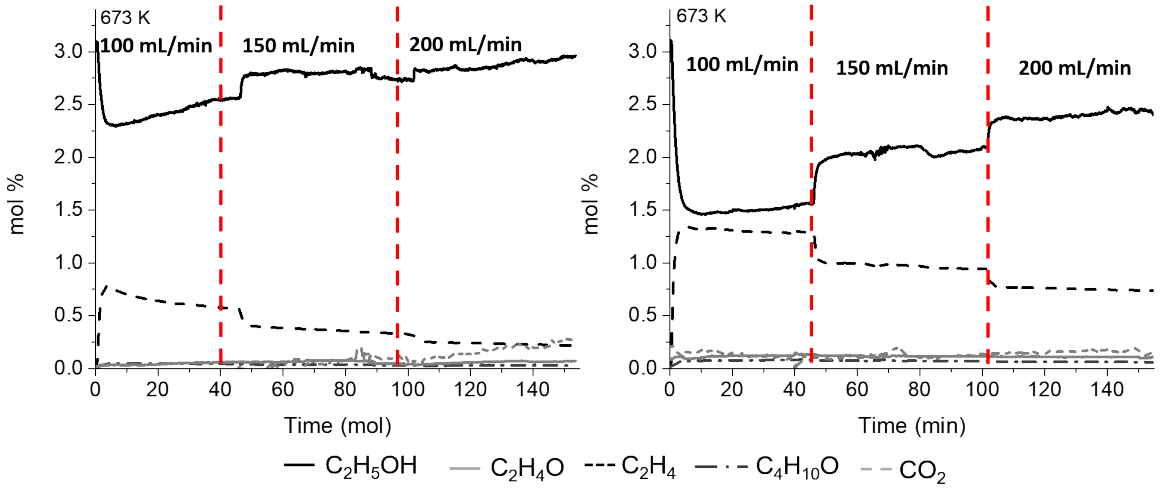

Figure 13. 2.5Nb2.5PSi left, 5Nb2.5PSi right, 3% EtOH at 673 K.

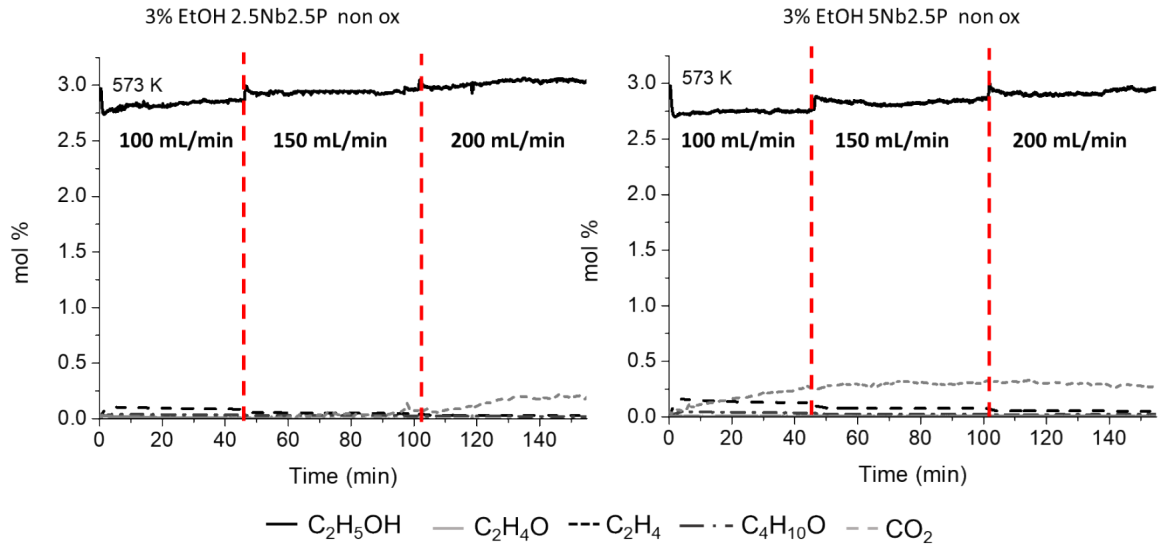

Figure 14. 2.5Nb2.5PSi left, 5Nb2.5PSi right, 3% EtOH at 573 K.

3.6 Evaluation of the apparent activation energy and reaction order for the ethanol dehydration to ethylene

From the catalytic data obtained at low conversion, and in absence of other products in that regime (in particular only traces of diethylether) it is possible to evaluate the kinetic parameters of reaction (1) over these catalysts. The apparent activation energy can be evaluated from the conversion data at different temperatures: the obtained values are 111 kJ/mol and 133 kJ//mol for 2.5Nb2.5Psi and 5Nb2.5Psi, respectively. These data are compared with difficulty with literature data, because over most catalysts the dehydration reaction to diethylether (reaction 3) is far faster than that to ethylene (reaction 1) at low temperature: this makes difficult the evaluation of the activation energy of reaction 1 at low temperature and conversion. However, it can be compared with values calculated for the reaction (1) supposed to be realized in the protonic acid H-MOR zeolite: in this case very small value 146.0 and 177.2 kJ/mol are reported for two different mechanisms [32]. In any case these apparent activation energy data indicate that our experiments are realized under chemical kinetic control, as they do also in the case of the experiments realized in oxidizing atmospheres, where apparent activation energy values around 90 kJ/mol are measured for ethanol conversion.

From the conversion data using different feed concentrations, the reaction order measured in steady state conditions is in the range 0.1-0.5 for both catalysts at 673 K. Such a slightly positive reaction order confirms that ethanol adsorption is very strong and that active sites are almost saturated in these conditions.

3.7 In-situ FT-IR study of ethanol adsorption and conversion.

Ethanol adsorption and thermal evolution at the catalyst surfaces, as well as the parallel formation of gas phase species, have also been also investigated as a function of the temperature in static conditions in an IR cell using a catalyst pressed disk.

In Fig.15 (left panel), the surface species spectra recorded after ethanol adsorption over sample 2.5Nb2.5PSi show the typical bands of CH deformation modes centered at 1482, 1450, 1397, 1383 sh, 1358 cm^{-1}. The corresponding CH stretching modes at 2981, 2940 split, 2910, and 2885 cm^{-1} are reported in in the inserts.

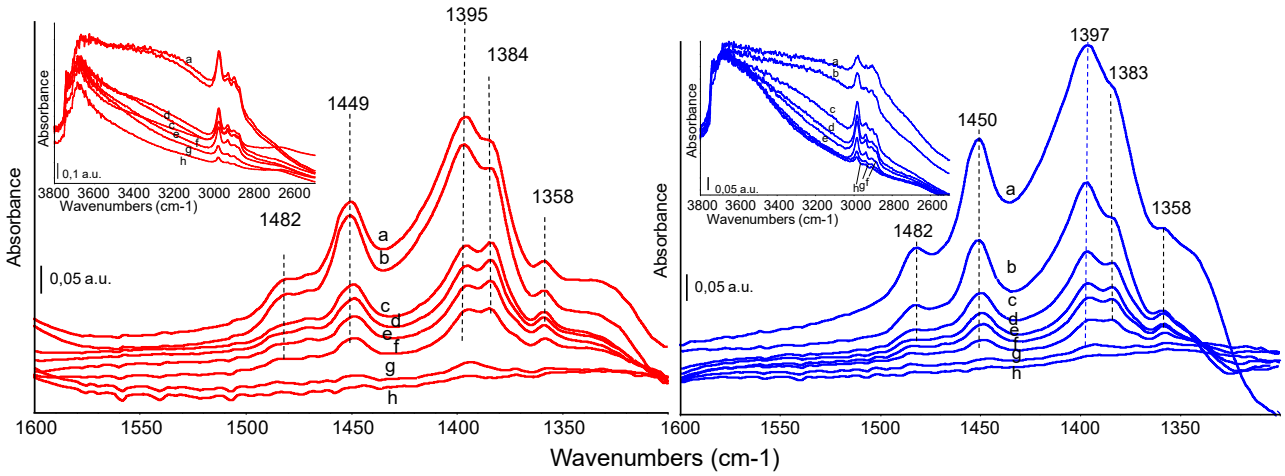

Figure 15. FT-IR subtraction spectra of surface species arising from ethanol adsorption and thermal evolution over sample 2.5Nb2.5PSi (left) and 5Nb2.5PSi (right). In ethanol at room temperature (a), after short outgassing at room temperature (b), 423 K (c), 473 K (d), 523 K (e), 573 K (f), 623 K (g), 673 K (h). The activated surface spectrum has been subtracted. In the inserts: unsubtracted spectra in the OH and CH stretching region.

CH stretching and deformation bands are detected almost unchanged in shape and position and progressively decreasing in intensity in the overall temperature range up to 573 K, while at 623 K they essentially disappear. A small change in relative intensities can be detected for the split band in the range 1390-1370 cm^{-1}. This band is assigned to symmetric bending modes of the CH_3 group and its splitting could be due to the formation of different adsorbed species. In the inserts, the behavior of OH stretching bands can be observed. While the complex absorptions in the 3800-3500 cm^{-1} region are due to surface hydroxy groups of the catalysts, as discussed above, the very broad absorption centered around 3200 cm^{-1} is likely due to the OH stretching mode of adsorbed undissociated ethanol. This absorption is essentially disappeared at 473 K, suggesting that at this temperature the residual bands are due to adsorbed ethoxy-groups. No information can be obtained by the analysis of the low

frequency region, i.e. the CO/CC stretching region, masked by the strong absorptions of the silica lattice.

The splitting of the CH_3 bending mode and the different behavior of the two components under outgassing and at increasing temperatures suggests that they are due to two different types of ethoxy groups, e.g. bonded to silica and to Nb and/or P atoms, i.e. weakly adsorbed and strongly adsorbed). Negative bands in the OH stretching region appearing in the subtraction spectra (not reported) provide evidence of the interaction of ethanol or ethoxy groups with the hydroxyl groups.

A very similar behavior characterizes ethanol adsorption and conversion over the 5Nb2.5PSi system (Fig. 15, right panel).

In Fig. 16 gas phase spectra recorded at increasing temperatures within the same experiment are reported and exemplified for sample 5Nb2.5PSi. In the gas phase spectra bands of residual and desorbed ethanol vapor (EtOH) are detected up to 473 K. Starting from this temperature, new features appear in the spectrum recorded at 523 K: a rotovibrational band at 950 cm^{-1} (PQR profile, $=CH_2$ wagging mode) assigned to ethylene and a weak band at 1135 cm^{-1} assigned to diethylether DEE (CO stretching mode).

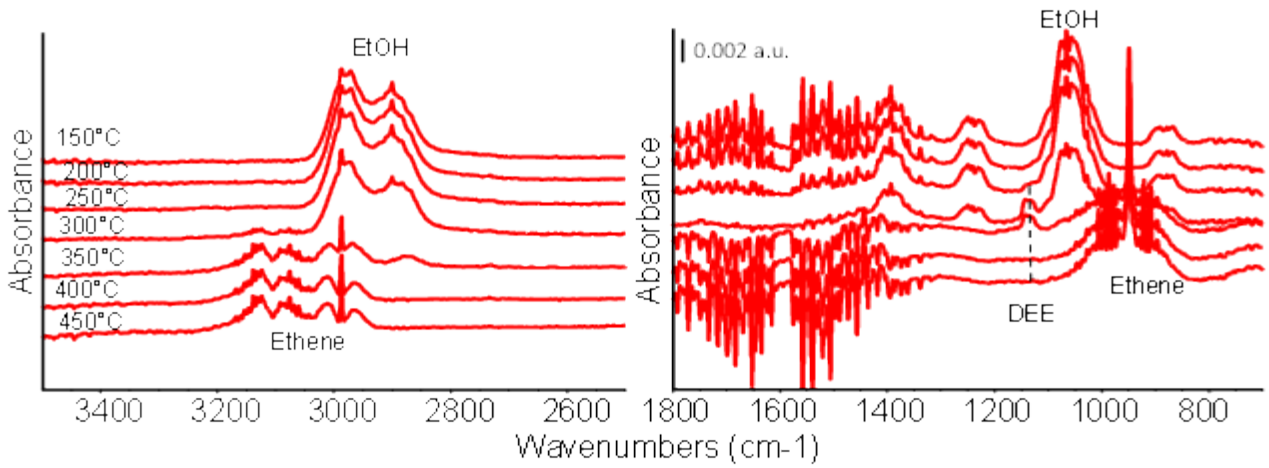

Figure 16. Gas phase species arising from ethanol thermal evolution over catalyst 5Nb2.5PSi.

At 573 K other bands can be clearly detected, consistent with the formation of ethylene (2990 cm^{-1}, CH stretching mode, 3108 cm^{-1}, $=CH_2$ stretching mode) and ether (2870 cm^{-1}, CH stretching mode, and 1100 cm^{-1}, C-O stretching mode).

Comparing band intensities, on both catalysts diethylether is already detected in traces at 523 K and peaks at 573 K, whereas ethylene starts to be detected in traces at 523 K and its

amount still increases up to 673 K. Almost complete ethanol conversion is observed between 573 and 623 K. Interestingly, while the general behavior of the two catalysts is definitely similar, the temperature at which ethanol is disappeared is slightly higher for the 2.5Nb2.5Psi catalyst (623-673 K, Fig. S4) than for the 5Nb2.5PSi catalyst, which appears to be the most active in ethanol dehydration in agreement with the above catalytic data and the quantitative determination of total acid sites, discussed above.

It is relevant to remark that, while diethylether is almost not observed in catalytic experiments, also at very low ethanol conversion, small amounts of it are observed in the spectroscopic experiments. It is however to be noted that also this experiment, compared with those realized with other catalysts [**Error! Bookmark not defined.**,**Error! Bookmark not defined.**], reveal the very weak activity of these catalysts in producing diethylether. On the other hand, diethylether does not appear at lower temperature than ethylene (as found on most catalysts) but at the same temperature as ethylene. Thus, this result can be taken as a confirmation that diethylether over these catalysts does not firm by ethanol dehydration reaction (3) but by ethanol addition to ethylene, reaction (4), as supposed above on the basis of steady state conversion experiments at different contact times.

The small amounts of diethylther formed in the 523 – 623 K temperature range, is cracked back either by the inverse of the same reaction (4), more favored at higher temperatures, or by reaction

$(CH_3CH_2)_2O \rightarrow 2\ H_2C{=}CH_2 + H_2O$ (5)

occurring above 623 K.

To collect more information, in the same conditions, adsorption and thermal evolution of diethylether have been tested over the most active catalyst, 5Nb2.5PSi. IR spectra of adsorbed species and gas phase species are reported in Fig. 17. In the spectra of the catalyst surface, bands at 1450 and 1390 cm^{-1} are due to the asymmetric and symmetric CH deformation modes of the CH_3 group. CH_2 deformation modes are evident at 1470 and 1350 cm^{-1} (figure 17A). Correspondingly, the CH stretching bands are detected in the high frequency region of the spectra at 2982, 2940, 2900 (sh) and 2884 cm^{-1} (Fig. S5). Above 573 K a very weak band can be observed just below 1700 cm^{-1} and likely assigned to traces of adsorbed carbonyl compounds such as acetaldehyde. The persistence of the band at 1350 cm^{-1}, which is not observed with adsorbed ethanol, suggests that the adsorbed species are constituted mainly by intact diethylether. These features are progressively weakened following temperature evolution up to 623 K, but no changes in position can be detected.

The analysis of gas phase spectra evidences ethylene formation between 523 and 573 K (Fig. 17B) that further increases until complete diethylether conversion at 723 K. No other reaction products are detected in these conditions. This indicates that diethylether cracking occurs through reaction (5) more than through the inverse of reaction (4), taking into account that in the conditions reaction (1) is already occurring fast.

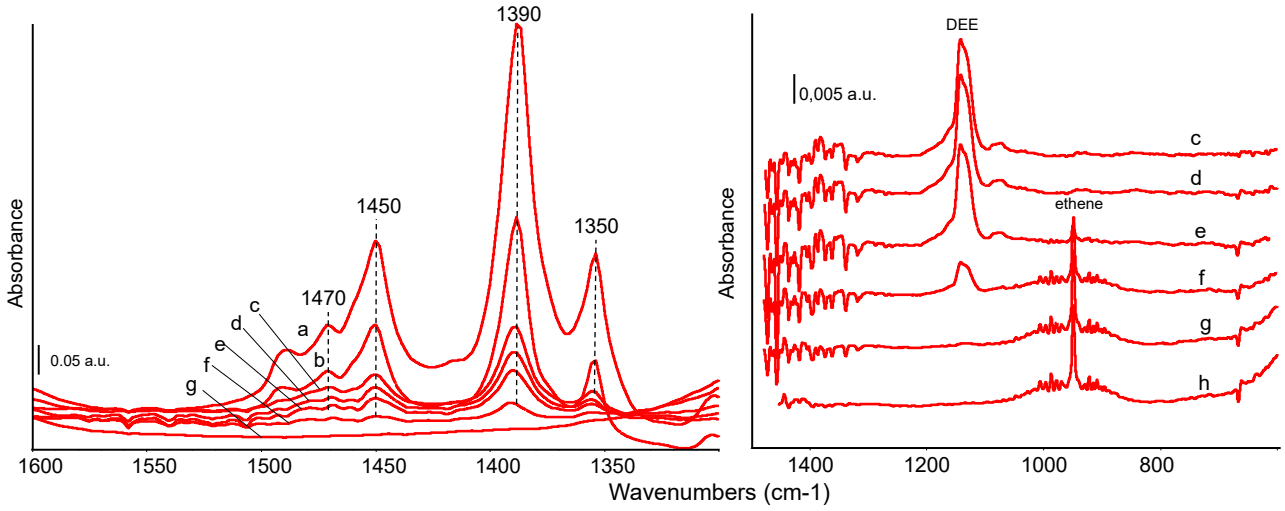

Figure 17. FT-IR subtraction spectra of surface species arising from DEE adsorption and thermal evolution over 5Nb2.5PSi catalyst (A) and corresponding gas phase species (B). In DEE at room temperature (a) and after short outgassing at room temperature (b), at 473 K (c), at 523 K (d), 573 K (e), 623 K (f), 673 K (g), 723 K (h). The activated surface spectrum has been subtracted from spectra in (A).

Pyridine adsorption has been carried out over the “spent” surface of 5Nb2.5PSi catalyst after reaction of ethanol in the IR cell and leads to spectra consistent with those reported in the previous paragraphs for the fresh sample (Fig. S5). The intensity ratio B/L signals (i.e. I_{1545}/I_{1610}) is slightly higher in the sample after ethanol conversion. New Brønsted sites might be formed also by production of water vapor during the reaction itself, but on the other side Lewis sites can be poisoned by coke formation.

Conclusions

The results of this study show that gel-derived Nb_2O_5-P_2O_5-SiO_2 solids are effective acidic catalytic materials with high-surface area and a combination of mesoprosity and microporosity. The samples retain S_{BET} surface areas ~ 350 m^2/g after calcination at 773 K. IR experiments show the presence, on the surface in the vacuum/solid interface, of hydroxy groups typical of silica-based materials (silanol groups), but also P-OH and/or Nb-OH

groups. IR studies of adsorption of pyridine in the gas/solid interface demonstrate that the samples show Brønsted acidity sufficiently strong to protonate this basic probe molecule, as well as medium-strong Lewis acidity similar to that previously found over niobia, thus reasonably attributed to Nb^{5+} coordinatively unsaturated centers.

These features are confirmed by ammonia adsorption and thermodesorption experiments, allowing to calculate the amount of strong and weak acid sites at the gas/solid interface. Furthermore, the PEA adsorption experiments performed at the liquid-solid interface show the higher acidity of the sample which is richer in niobium and possesses also mesoporosity. In all cases it is confirmed that the increased amount of niobia results in an increase of the concentration of surface acid sites, although the additional sites are weaker than those present in the lower-Nb-content sample.

Catalytic experiments, realized both in the Temperature Programmed Reaction mode, and in steady state conditions, reveal medium-high catalytic activity of the ternary oxides in the gas-phase acid-catalyzed conversion of ethanol to ethylene, starting from around 500 K, with a minimal or no formation of diethylether also at low temperature and ethanol conversion. Traces of diethylether form at higher contact times suggesting that it is a secondary product formed by addition of ethanol to ethylene. However, the two catalysts also show parallel activity in ethanol dehydrogenation to acetaldehyde, which is only weakly affected by the presence of oxygen in the gas phase. The sample richer in niobium is more active, as expected indeed. Some catalyst deactivation is found, which is more significant at low temperature and for the sample with less niobium.

IR spectra confirm the data of catalytic experiments, showing the formation of strongly adsorbed alkoxide species, that decompose to ethylene above 523 K. Overall, these catalysts appear very promising for the production of bioethylene from bioethanol without a minimal coproduction of diethylether.

References.

[1] G. Busca, A. Gervasini, Advan. Catal., C. Song ed., vol. 67 (2020) 1-90.

[2] G. Busca, Micropor. Mesopor. Mat., 254 (2017) 3-16.

[3] G. Busca, Chem. Rev., 107(2007) 5366-5410

[4] G. Busca, Phys. Chem. Chem. Phys., 1, 723-736 (1999)

[5] F. Cavani, G. Girotti, G. Terzoni, Appl. Catal. A Gen., 97 (1993) 177-196.

[6] V.N. Ipatieff, R.E. Schaad, Ind. Eng. Chem. 30 (1938) 596-599.

[7] I. Nowak, M. Ziolek, Chem. Rev., 99 (1999) 3603–3624.

[8] G. Busca, G. Ramis, V. Lorenzelli, P.F. Rossi, A. La Ginestra, P. Patrono, Langmuir, 5 (1989) 911-916

[9] M.J. Campos Molina, M. López Granados, A. Gervasini. P. Carniti, Catal. Today, 254 (2015) 90-98.

[10] P.A. Burke, E.I. Ko, 129 (1991) 38-46.

[11] J.L. Vieira, G. Paul, G.D. Iga, N.M. Cabral, J.M.C. Bueno, C. Bisio, J.M.R. Gallo, Appl. Cat. A, Gen. 617 (2021) 118099.

[12] Q. Liu, H. Liu, D.-M. Gao, Chem. Eng. J. 430 (2022) 132756

[13] N.J. Clayden, G. Accardo, P. Mazzei, A. Piccolo, P. Pernice, A. Vergara, C. Ferone, A. Aronne, J. Mater. Chem. A, 3 (2015) 15986–15995.

[14] A. Gervasini, S. Campisi, P. Carniti, M. Fantauzzi, C. Imparato, N.J. Clayden, A. Aronne, A. Rossi, Appl. Catal. A, 579 (2019) 9–17.

[15] A. Aronne, M. Di Serio, R. Vitiello, N.J. Clayden, L. Minieri, C. Imparato, A. Piccolo, P. Pernice, P. Carniti, A. Gervasini, J. Phys. Chem. C, 121 (2017) 17378–17389.

[16] A. Gervasini, P. Carniti, F. Bossola, C. Imparato, P. Pernice, N.J. Clayden, A. Aronne, Mol. Catal., 458 (2018) 280–286.

[17] N.J. Clayden, C. Imparato, R. Avolio, G. Ferraro, M.E. Errico, A. Vergara, G. Busca, A. Gervasini, A. Aronne, B. Silvestri, Green Chemistry, 22 (2020) 7140-7151

[18] S. Ross, J.P. Olivier, On Physical Adsorption, Wiley and Sons, New York, (1964).

[19 K. Hadjiivanov, Advan Catal., F.C. Jentoft ed., 57 (2014) 99-318.

[20] T. Armaroli, G. Busca, C. Carlini, M. Giuttari, A. M. Raspolli Galletti, G. Sbrana, J. Mol. Catal., 151, 233-243 (2000)

[21 H.Gomez Bernal, A. M. Raspolli Galletti, G.Garbarino, G.Busca, E.Finocchio, Applied Catalysis A: General, 502 (2015) 388-398.

[22] G. Busca, Catal. Today 41 (1998) 191-206

[23] G. Busca, Progr. Mater. Sci. 104 (2019) 215-249.

[24] G. Busca, Phys. Chem. Chem. Phys., 1 (1999) 723-736

[25] C. Carlini, M. Giuttari, A. M. Raspolli Galletti, G. Sbrana, T. Armaroli and G. Busca, Appl. Catal., A Gen., 183, 295-302 (1999)

[26] M. Massa, A. Andersson, E. Finocchio, G. Busca, J. Catal. 307 (2013) 170–184

[27] G. Ramis, P.F. Rossi, G. Busca, V. Lorenzelli, A. La Ginestra and P. Patrono, Langmuir, 5, 917-922 (1989)

[28] K. Nakajima, Y. Baba, R. Noma, M. Kitano,J.N. Kondo, S. Hayashi, M.Hara, J. Am. Chem. Soc. 133 (2011) 4224–4227

[29] V. Sanchez Escribano, G. Garbarino, E. Finocchio, G. Busca, Top. Catal 60 (2017) 1554–1564.

[30] T. K. Phung, G. Busca, Chem. Eng. J. 272 (2015) 560-567.

[31] G. Garbarino, R. Prasath Parameswari Vijayakumar, P. Riani, E. Finocchio, G. Busca, Appl. Catal. B Environ. 236 (2018) 490-500.

[32] H. Xia, ACS Omega 2020, 5, 9707−9713

Surface Acid Properties of Nb_2O_5-P_2O_5-SiO_2 Gel-Derived Catalysts

Gabriella Garbarino[1], Giovanni Pampararo[2], Elisabetta Finocchio[1], Guido Busca[1*], Antonella Gervasini[3], Sebastiano Campisi[3], Brigida Silvestri[4], Claudio Imparato[4], Antonio Aronne[4*]

[1] Dipartimento di Ingegneria Civile, Chimica e Ambientale, Università di Genova, Via Opera Pia 15, I-16145 Genova, Italy.
[2] Dipartimento di Chimica e Chimica Industriale, Università di Genova, Via Dodecaneso 31, I-16146 Genova, Italy
[3] Dipartimento di Chimica, Università degli Studi di Milano, Via Camillo Golgi 19, I-20133 Milano, Italy.
[4] Dipartimento di Ingegneria Chimica, dei Materiali e della Produzione Industriale, Università di Napoli Federico II, P.le Tecchio, 80, I-80125, Napoli, Italy.

*Corresponding authors: anaronne@unina.it; guido.busca@unige.it

Abstract

Amorphous catalytic materials belonging to the Nb_2O_5-P_2O_5-SiO_2 system were prepared through an original sustainable sol-gel procedure, and characterized by surface area, porosity and acidity measurements. Their acid properties have been investigated by FTIR spectroscopy of adsorbed pyridine, ammonia titration and TPR, as well as by titration with 2-phenylethylamine from organic solution. They present Lewis acidity attributed to niobium surface cationic centers, and Brønsted acidity sufficiently strong to protonate pyridine. The total acidity depends on the niobium content. The conversion of ethanol was investigated by vapor phase Temperature Programmed Reaction, steady-state catalytic experiments and static In Situ FTIR experiments. The samples are active in converting ethanol to ethylene with 100 % selectivity at low conversion (523-573 K), but also produce acetaldehyde by dehydrogenation at higher temperature and conversion. They show an unusually poor activity for the production of diethylether also at low ethanol conversion. Ethoxy groups act as reaction surface intermediates.

Keywords: acid solids; sol-gel; ethanol dehydration; niobia; phosphoric anhydride.

1. Introduction

Solid acid catalysts play a very relevant role in industrial chemistry [1]. Very strong acidic materials, such as protonic zeolites [2], are mostly needed to activate very weak σ-type bases such as paraffins as well as quite electron deficient π-type bases such as e.g. ethylene for alkylation reactions. Indeed, these materials play a key role in the refinery and petrochemistry fields [3]. Weaker protonic solid acids [4], such as e.g. the so called "solid phosphoric acid" catalyst (SPA) [5,6], can also be applied for less demanding reactions, e.g. for protonation of more electron-rich olefins to produce oligomerization or aromatic alkylations. Moderately strong protonic solid acids, and Lewis acids as well, may be even more performant in activating stronger n-type bases, such as oxygenates, and for this reason they may play an even more important role in the renewable industrial chemistry based on biomass conversions. For this application, acid water tolerant catalytic materials are also needed, since they are generally employed in aqueous solution or exposed to humidity. In these processes, niobium and phosphorus-based catalysts are widely used owing to tunable distribution of both Brønsted and Lewis acidic sites combined with high stability towards hydrolysis given by Nb–O–P bonds [7]. In particular, the niobium-phosphorus-silicon mixed oxide systems emerged as an environmentally friendly and performant system for biomass conversion. Previous studies showed that, while silica is characterized by low surface protonic acidity, P_2O_5 provides significantly stronger Brønsted acidity [8] while niobia provides both Brønsted and Lewis acidity [9,10,11,12].

A hydrolytic sol–gel procedure was developed by some of the authors to synthesize Nb_2O_5–P_2O_5–SiO_2 (Nb-P-Si) materials [13,14] which were proved to be effective catalysts in dehydration of fructose, hydrolysis of inulin and esterification of oleic acid with polyalcohols for biolubricant production [15,16]. The proper incorporation of a niobium phosphate phase into a silica matrix allows a fine dispersion of acid sites over a large surface area, even with relatively low amounts of Nb and P, with highly stable anchorage of phosphorous into the matrix.

In this scenario, following the principles of sustainable chemistry, a new chloride-free sol–gel procedure has been recently performed using ammonium niobium oxalate and phosphoric acid as both precursors and acid catalysts, water as solvent and no additional mineral acid catalysts. The obtained ternary oxides showed, according to a preliminary investigation, promising acid-type catalytic activity [17]. The aim of the present work is a

more extensive assessment of the acidic properties of this family of catalytic materials in terms of strength, distribution and accessibility of acid sites. Moreover, the reactivity of the samples towards ethanol was studied by spectroscopic analyses and ethanol temperature programmed surface reaction. The product distribution observed allows to confirm the potentiality of the samples as selective acidic catalysts.

2. Experimental

2.1 Synthesis procedure

Niobium–phosphorus–silicon mixed oxide materials were prepared by a hydrolytic sol–gel synthesis following our previously reported procedure [17]. Tetraethoxysilane, $Si(OC_2H_5)_4$, TEOS, (98%, Sigma- Aldrich), phosphoric acid (85 wt% solution, AppliChem), ammonium niobium oxalate hydrate, $NH_4[NbO(C_2O_4)_2(H_2O)_2]\cdot nH_2O$, ANbO (kindly supplied by Companhia Brasileira de Metallurgia e Mineração, CBMM), were used as precursors.

Sample with two different molar compositions were synthesized: $2.5Nb_2O_5\cdot 2.5P_2O_5\cdot 95SiO_2$ and $5Nb_2O_5\cdot 2.5P_2O_5\cdot 92.5SiO_2$, indicated in the following as 2.5Nb2.5PSi and 5Nb2.5PSi, respectively. Briefly, a proper amount of ANbO was added to a mixture of TEOS and deionized water, followed by the addition of H_3PO_4, then the system was stirred at room temperature until gelation occurred. The gels were dried in air up to 383 K in an air-ventilated oven and then the dried gels were annealed in a tube furnace under air flow at 773 K for 1 h with a heating rate of 10 K min^{-1}. Experimental details about the synthesis procedure are reported in the Supplementary material.

2.2 Morphological characterization

N_2 adsorption and desorption isotherms were collected at liquid nitrogen temperature (77 K) on an automatic analyser of surface area (Sorptomatic 1990 version instrument from Thermo Scientific Carlo Erba). Before the experiments, fresh and treated samples at 573 K and 773 K (maintained for 1 h) were outgassed at 423 K for 16 h (ca., 0.15 g, 80-200 mesh). Surface area values were computed from 3-parameters BET equation in the range $0.05<p/p_0<0.4$. Microporous volume and micropore size were calculated using Saito and Foiley (S-F) model in the interval $0<p/p_0<0.35$ using the nitrogen on zeolite potential-function [18]. Conventional BJH model was used for mesoporosity determination. The adsorbed volume, expressed in cm^3 (STP) $\cdot g^{-1}$, was converted into pore volume, $cm^3\cdot g^{-1}$, considering the density of N_2 in the normal liquid state ρ =0.8081 g $cm\cdot g^{-1}$); molecular area of N_2 was taken as 16.2 $Å^2$.

2.3 Surface acidity studies

Qualitative characterization of the surface acid sites at the vapor/solid interface was realized by a FT-IR study of adsorbed pyridine. Experiments have been performed in a conventional home-made glass cell with KBr windows, connected to a gas manipulation apparatus. A simplified sketch of the experimental apparatus is reported in Supplementary Information (figure S1) [19]. Before any adsorption experiment, samples have been activated in vacuum (10^{-3} torr) for one hour at 753 K (i.e. below calcination temperature). In a specific case, activation temperature was set at 823 K, as indicated in the discussion section. Sample powders have been pressed in disks of 13 mm diameter, 15 mg average weight.

Pyridine adsorption (2 torr vapor) was performed at room temperature and following outgassing at increasing temperatures. Spectra of the pure powder disks were recorded at each adsorption/desorption step, using a Thermonicolet Nexus instrument (4 cm^{-1} resolution, 100 scans, OMNIC software). The reference (background) spectrum was the empty cell. The reported subtraction spectra are obtained by subtracting the spectrum of the activated catalyst surface (i.e. after outgassing at high temperature) from the spectrum of the catalyst after vapor adsorption.

Gas-solid titrations were performed by NH_3 probe adsorption in flowing dynamic experiments in a home-made adsorption line equipped with mass flow controllers for gas flow regulation, an electrical vertical oven for temperature control and linked to a FT-IR spectrophotometer (Bio-Rad with DTGS detector) (see Fig. S2). A quartz reactor packed with pellets of the sample (*ca*. 0.1 g, particles in the range of 80-200 mesh dried at 373 K overnight) was placed inside the oven. The samples were pre-treated at 393 K under flowing nitrogen for 30 min. prior to the measurements in order to desorb impurities and remove physically adsorbed water. Then, a NH_3/N_2 mixture, with NH_3 concentration of *ca*. 500 ppm flowed at 4 NL h^{-1} through the reactor maintained at 393 K. The gas flow at the outlet of the reactor entered in a gas cell (path length 2.4 m multiple reflection gas cell) in the beam of the FT-IR spectrophotometer where it was measured online (monitoring NH_3 line at 966 cm^{-1}, N-H asymmetric stretching, wagging mode). The number of acid sites (in $\mu equiv \cdot g^{-1}$) was determined by quantitatively evaluating the adsorbed NH_3.

Thermo-desorption analysis of ammonia (NH_3-TPD) was carried out on NH_3-saturated samples by operating in the line above described. Approximately 60 mg of sample (80-200 mesh particle size) was pre-treated in the quartz tubular sample-holder at 393 K for 30 min under N_2 flowing at 50 $ml \cdot min^{-1}$. Ammonia saturation was achieved by flowing 1% NH_3/N_2

at 50 ml·min^{-1} for ca. 50-60 min at 298 K. The adsorbed NH_3 was monitored following continuously the NH_3 line at 966 cm^{-1} as a function of time. After attainment of saturation, at first, an isothermal step at 423 K was performed under N_2 flowing (50 ml·min^{-1}) to remove the excess of adsorbed ammonia from the surface (physisorbed) until attainment of a stable signal. Then, temperature was raised at 10 K·min^{-1} up to 1073 K and TPD spectrum was recorded, see Fig. S3.

Acid site titrations in solid-liquid phase using 2-phenylethylamine (PEA) as probe were carried out in a recirculation chromatographic line (HPLC), consisting of a pump (Waters mod. 515) and a monochromatic UV detector (Waters mod. 2487, working at fixed λ = 254 nm), coupled to a personal computer for the collection, storage, and processing of the data. Some details are reported in the supplementary information (page 3). The samples (ca. 0.03 g, crushed and sieved as 80-200 mesh particles) were placed between two sand pillows in a stainless steel sample-holder (length 12 cm, i.d. 2 mm) mounted in place of the chromatographic column and surrounded by a glass jacket thermostated by circulating water (303.0±0.1K). Before each experiment, the sample underwent a thermal pre-treatment (423 K in 8 mL min^{-1} air flux for 16 h) and then it was conditioned in the same solvent employed as eluent (cyclohexane).

A first adsorption was performed by repeatedly injecting successive dosed amounts of PEA solution (50 µL, ca. 0.10 M) into the chromatographic line. A step-chromatogram was obtained, where each step represents the achieving of adsorption equilibrium. First adsorption was considered concluded, when at least three successive injections gave identical step height in the chromatogram, indicating that saturation was attained and no sites were available for PEA adsorption. After the collection of the first adsorption isotherm on fresh sample (I° run), pure solvent flowed through the saturated sample overnight (ca. 16 h), thus permitting desorption of the probe molecules from weakly interacting sites. Then, a second adsorption of PEA on the same sample was repeated (II° run) to titrate weak acid sites and evaluate strong acid sites by difference.

2.4. Studies of the surface reactivity towards ethanol

2.4.1 Ethanol Temperature Programmed Surface reaction (EtOH-TPSR)

Ethanol surface programmed surface reaction were conducted in a continuous fixed bed reactor (6 mm internal diameter) in non-oxidative and oxidative environments. In each experiment, 43 mg of the un-sieved sample were mixed with 127 mg of calcined sand (60-70 mesh 274739 from Sigma-Aldrich, stabilized at 1073 K for 5 h). The temperature was

increased (373-773 K) with a ramping rate of 5 K/min, and, at the end, the maximum temperature of 773 K was kept constant for 15 minutes.

For non-oxidative experiments, either 1 mol% or 2.5 mol% of ethanol in pure nitrogen was fed at the flow rate of 170 NmL/min. For the experiments in oxidative conditions the feed was 1 mol% EtOH/6% O_2/93% N_2, i.e. with an oxygen content sufficient to obtain full ethanol combustion. In all cases, the GHSV is around 220000 h^{-1}. The product analysis was realized by continuous online FT-IR analysis (Nicolet 380 FT-IR spectrometer) equipped with a home-made gas cell and accurate calibration for all observed molecules, i.e. ethanol, diethylether, carbon dioxide, ethylene and acetaldehyde using their specific absorptions.

2.4.2 FT-IR studies of ethanol adsorption and reactivity

Ethanol adsorption experiments have been performed in situ, in static conditions, in the same apparatus and instrument described above for pyridine adsorption (figure S2, transmission mode). Catalysts powder disks have been prepared in the same way, too. Samples have been activated in vacuum for one hour at the reported temperature in the oven connected to the IR cell and the gas manipulation apparatus. The adsorption step has been carried out at room temperature, with the sample placed the IR cell outside the heated zone. Ethanol vapor was admitted to the sample in the cell up to a pressure of 2 torr, then the cell was outgassed down to ethanol pressure lower than 1 torr (around 0.2 torr). Catalyst disks have then been heated in the oven in the presence of residual ethanol vapor and, at each temperature, spectra of gas phase species as well as spectra of the catalyst surface “quenched” at room temperature have been recorded.

In a first step, two spectra were recorded: catalyst in the presence of ethanol vapor and after short outgassing at room temperature applied in order to have only some residual ethanol vapor in gas phase (< 1 torr). After this step, thermal evolution of both adsorbed and gas phase species was studied in static conditions and in the range 423-723 K, by recording spectra of the surface and of the gas phase species.

2.5 Ethanol conversion catalytic experiments.

Steady state experiments were carried out in oxidative environment in the same conditions used in Oxidative Ethanol TPSR. Catalytic material was loaded with a higher amount of sand (43 mg catalyst powder in 300 mg of sand) in order to avoid non-isothermal behavior in the catalytic bed. Temperature is increased step by step from 373 to 773 K, with a temperature interval of 50 K and a dwelling time of 30 minutes.

To evaluate the effect of contact time, experiments were realized in non oxidative conditions (1 and 3 mol% ethanol in nitrogen), at relatively low temperatures, 673 K and 573 K.

Catalysts were diluted in sand (43 mg catalyst powder in 300 mg of sand). Three different space velocities were tested, obtained by varying the total flow rate, 100, 150 and 200 mL/min, corresponding to GHSV around 130000 h^{-1}, 190000 h^{-1} and 260000 h^{-1}.

3. Results and discussion

3.1 Morphology characterization.

It has been already shown [17] that the adopted sol-gel synthesis produced *water-tolerant* Nb-P-Si solid acids featuring a tunable distribution of Nb- and P-species in the silicate framework and the firm anchorage of P in the matrix. The materials look amorphous at XRD analysis (Fig. S4 in supplementary information), and, according to spectroscopic data, show a good homogeneity in elemental distribution [17]. The choice of ammonium niobium oxalate as precursor allowed the control of the Nb coordination number influencing the hydrolysis of Nb oligomers in the sol and in turn the distribution of Nb polyhedra in the gels. As derived from previously reported solid state NMR, FT-IR and Raman investigation [17] an amorphous silicate network including $NbOPO_4$ nanocrystals, already showing a high degree of cross-linking, was obtained in dried gels. During the thermal treatment at 773 K further self/cross-condensation reactions occurred between Nb-, P- and Si-units ultimately producing an amorphous structure composed of Nb–O–Si and/or Nb–O–Nb and P–O–Nb and/or P–O–P bridges. The calcination at high temperature did not negatively influence the morphological properties of the samples. Really, both dried and 573 K-calcined gels had surface area values only a little higher (10%-20%) than those calcined at 773 K (Table 1).

The detailed results on the morphological characterization of the calcined samples (773 K), 2.5Nb2.5PSi and 5Nb2.5PSi, based on the collected N_2 adsorption/desorption isotherms, are reported In Table 1. Both samples have N_2-adsorption/desorption isotherms typical of microporous solids (Type I, IUPAC classification), showing asymptotic trends typical of Langmuirian curves and absence of clear hysteresis (Fig. 1, a1 and b1).

Table 1. Morphological properties of the ternary oxidic samples

Sample	Total Surface Area[a] $m^2\ g^{-1}$	*Mesoporosity* [b]		*Microporosity* [c]	
		Pore $Size_{av}$ nm	Pore Volume $cm^3\ g^{-1}$	Pore $Size_{av}$ nm	Pore volume $cm^3\ g^{-1}$
2.5Nb2.5PSi	407 C_{BET}: 164 N_{av}:1.5	5.3	0.02	1.3	0.16
5Nb2.5PSi	365 $C_{BET:}$ 156 N_{av}: 2.6	3.4	0.06	1.6	0.17

[a] Obtained from the 3-parameters BET fit, in the $0.05 < p/p^0 < 0.4$ interval, ref. [17].
[b] Most representative pore population computed from B.J.H. model on the desorption isotherm branch in the $0.3 < p/p^0 < 0.95$ interval with standard universal isotherm (Harkins-Jura) (ASTM Standards Designation: D 4641-87)
[c] Calculated from p/p^0 0 to 0.35 with potential function: nitrogen on zeolite at 77 K, from literature [18].
C_{BET}.: Brunauer, Emmett, and Teller (BET) constant. N_{av}. average number of nitrogen molecule layers.

The 2.5Nb2.5PSi sample shows a more pronounced Langmuirian curve than 5Nb2.5PSi and, accordingly, the computed microporous size is smaller for 2.5Nb2.5PSi (1.3 nm) than for 5Nb2.5PSi (1.6 nm). Micropore distributions in the 0-4 nm range (pore radius) have been detailed for two samples in Fig. 1, a3 and b3. The presence of mesopores cannot be completely ruled out, actually BJH equation indicates poor mesoporous volume, as expected, associated with small mesopore size, of 5.3 nm for 2.5Nb2.5PSi and 3.4 nm for 5Nb2.5PSi. Then, from the morphologic analysis, it can be inferred that in both samples microporosity predominates over the mesoporosity. As concerns this latter, structural effect deriving from the presence of Nb oxide component, which acts as bridge between Si and P units, might be responsible for higher mesoporosity in 5Nb2.5PSi than 2.5Nb2.5PSi.
The values of surface area are similar to those previously reported for other Nb-P-Si samples [13,14]. The lower surface area value of 5Nb2.5PSi (365 $m^2 \cdot g^{-1}$) with respect to 2.5Nb2.5PSi (407 $m^2 \cdot g^{-1}$) is likely due to the lower amount of SiO_2, decreased from 84.8 wt.% to 76.7 wt%.

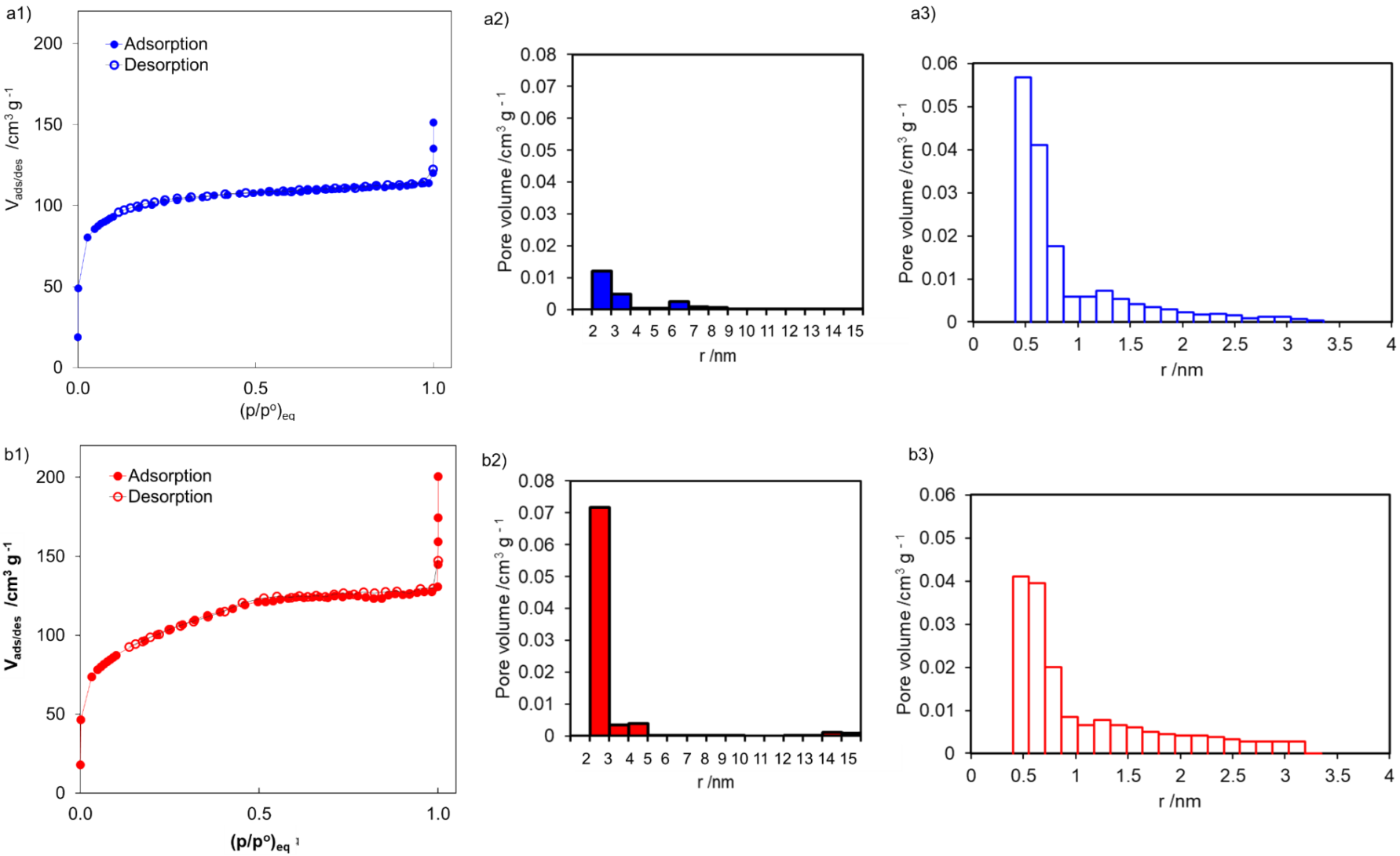

Figure 1. Morphologic characterization of 2.5Nb2.5PSi sample (a) and 5Nb2.5PSi (b) samples treated at 773 K. N_2 adsorption and desorption isotherms at 77 K (a1 and b1), mesopore size distribution determined by BJH model equation from the desorption branch of the N_2-isotherms (a2 and b2), and micropore size distribution determined by Saito and Foiley model equation (a3 and b3) [18].

3.2 Surface structure and acidity characterization

Qualitative analyses of the surface structure and surface acidity of the samples were realized using FT-IR spectroscopy of pure powder pressed disks at the vacuum/vapour/solid interface. The FT-IR spectrum of the 2.5Nb2.5PSi sample after outgassing at 763 K (Fig. 2, a) shows in the OH stretching region two main components, a broad and ill-defined absorption with two apparent maxima around 3700 and 3665 cm^{-1}, together with a sharper component centered near 3740-3720 cm^{-1}. The latter is associated to the presence of isolated silanol Si-OH species, typically located in that range [20], while the former component can be assigned to a combination of P-OH and Nb-OH groups [21,22]. After outgassing at 823 K, i.e. at temperature higher than the calcination temperature of these samples, a noticeable dehydration of the surface occurs, reducing the absorption in the whole region 3700-3200 cm^{-1}, in large part due to H-bonded OH groups (Fig. 2, b). Only silanols are still detected evidently (free and residual H-bonded silanols), while the other bands are only observable as shoulders. As expected, adsorbing few torr of water vapor admitted at room temperature in the IR cell over the same surface results in a reconstitution of hydroxyl groups other than free silanols characterized by a broad absorption centered near 3650 cm^{-1}, consistent with the attribution to P-OH species, and a very broad absorption centered around 3300 cm^{-1}, due to H-bonded water and hydroxy groups (Fig. 2, c).

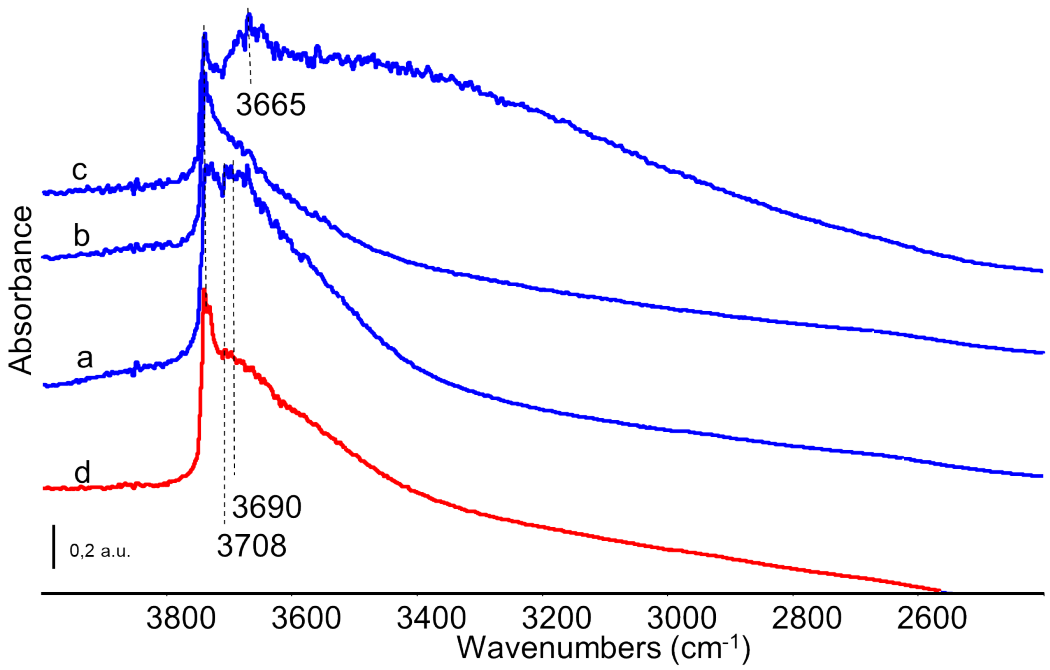

Figure 2. FT-IR spectra of samples in the OH stretching region. 2.5Nb2.5PSi sample (blue) after outgassing at 763 K (a), at 823 K (b) and after subsequent contact with 2 torr of water vapor (c). Spectrum of 5Nb2.5PSi sample (red) after outgassing at 763 K (d).

The spectrum of the 5Nb2.5PSi sample after outgassing at 763 K (Fig. 2, d) is very similar to that of the 2.5Nb2.5Si sample outgassed at 823 K, suggesting that the addition of more niobium oxide results in a stronger interaction or to condensation with the OH groups that are hydrogen bonded in the case of the lower Nb content sample.

The nature of the surface acidity has been investigated by FT-IR spectroscopy using pyridine as an adsorbed probe. Over the 2.5NbPSi sample (Fig. 3), pyridine adsorption and outgassing at room temperature evidences the presence of both molecularly adsorbed species and protonated species. Molecular species are characterized by the detection of the 8a vibrational modes at 1595 and 1609 cm^{-1}, and 19b vibrational mode at 1448 cm^{-1}, with a shoulder at lower frequencies. The shift of these bands to higher wavenumbers with respect to those reported for the free molecule (1583 and 1436 cm^{-1}, respectively) is an evidence of the interaction of these species with electron-withdrawing centers [23]. While the couple of bands at 1595 cm^{-1} and around 1440 cm^{-1} can be likely indicative of a medium-strong hydrogen bonding (as it may occur with the weakly acidic silanol groups), the bands at 1609 and 1448 cm^{-1} are certainly associated to the interaction with quite strong Lewis acid sites. The latter adsorbed species are still detectable up to 623 K and a very small shift towards higher frequencies at decreasing coverage is within the resolution of the instrument. Taking into account that tetravalent silicon (such as in silica and silicates [24]) and pentavalent phosphorous as well [25] are not able to provide Lewis acidity, these species would confirm the Lewis acidity of pentavalent niobium, as also found on the surface of pure niobic acid [26] as well as of niobia-silica [27].

The absorptions at 1638 and 1545 cm^{-1} are instead certainly due to pyridinium ion (8a and 19a modes [23]), thus they provide evidence of the presence of Brønsted acid sites. Brønsted acidic sites able to protonate pyridine are absent on pure silicas, while are present on P_2O_5-SiO_2 [28], Nb_2O_5-SiO_2 [27], niobic acid [26] and niobium phosphate [22], and are consequently to be attributed to Nb-OH and/or P-OH groups.

Thus, these data confirm the presence of Si-OH, Nb-OH and P-OH groups, free and H-bonded, and the presence of both Brønsted and Lewis acidity in the samples, as previously reported for differently prepared Nb-P-Si samples [14-16].

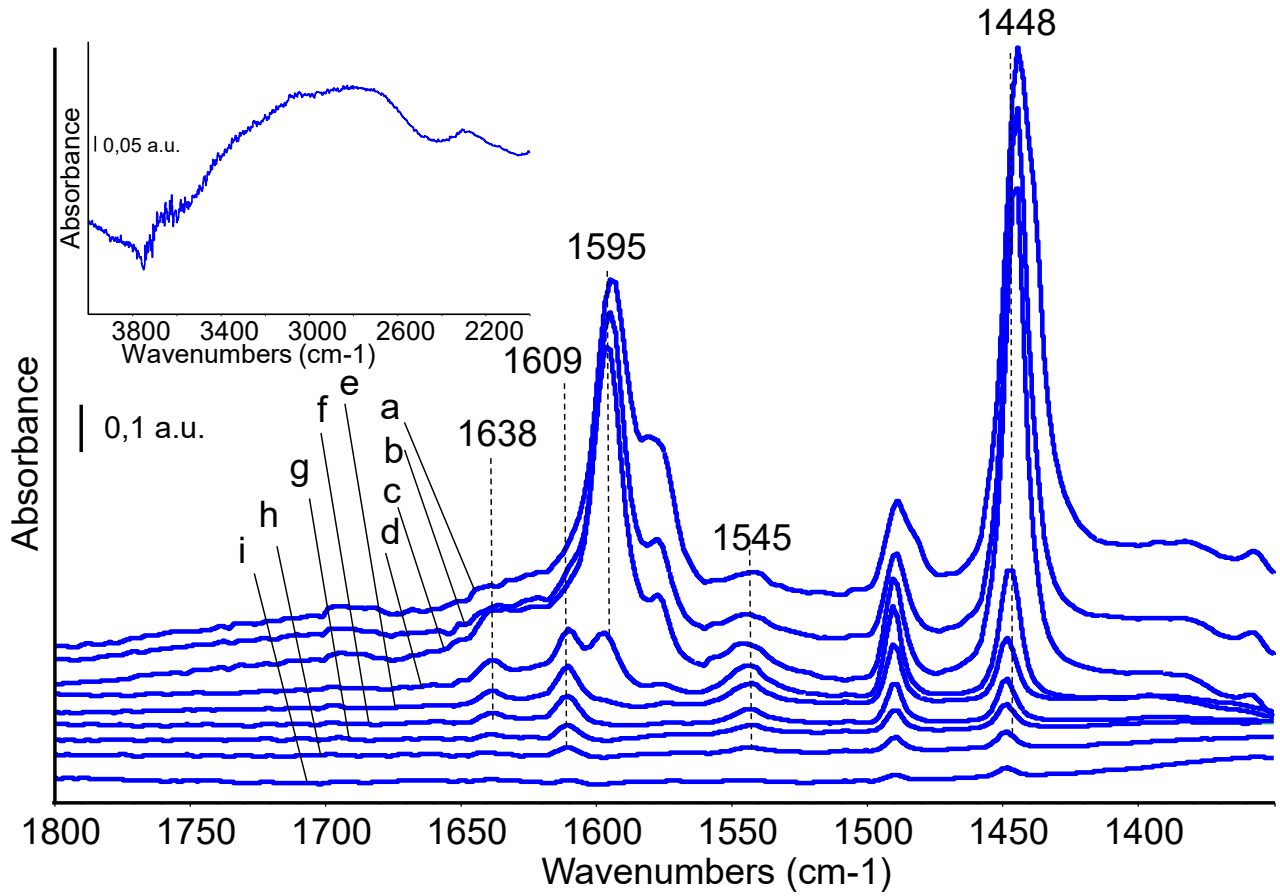

Figure 3. FT-IR subtraction spectra of adsorbed surface species arising from pyridine adsorption at room temperature over 2.5Nb2.5PSi sample (a) and after outgassing at room temperature (b), prolonged outgassing (40 min ca) at room temperature (c and inset: OH stretching region), outgassing at 423 K (d), 473 K (e), 523 K (f), 573 K (g), 623 K (h), 673 K (i). The activated surface spectrum has been subtracted.

Also over the 5Nb2.5PSi sample, pyridine adsorption and outgassing at room temperature (Fig. 4) provide evidence of the presence of both exposed Lewis sites and Brønsted sites, whose main diagnostic bands are located at 1608 cm^{-1} (shoulder, 8a vibrational mode of Lewis-bonded molecular pyridine) and 1545 cm^{-1} (19a mode of pyridinium ion), respectively.

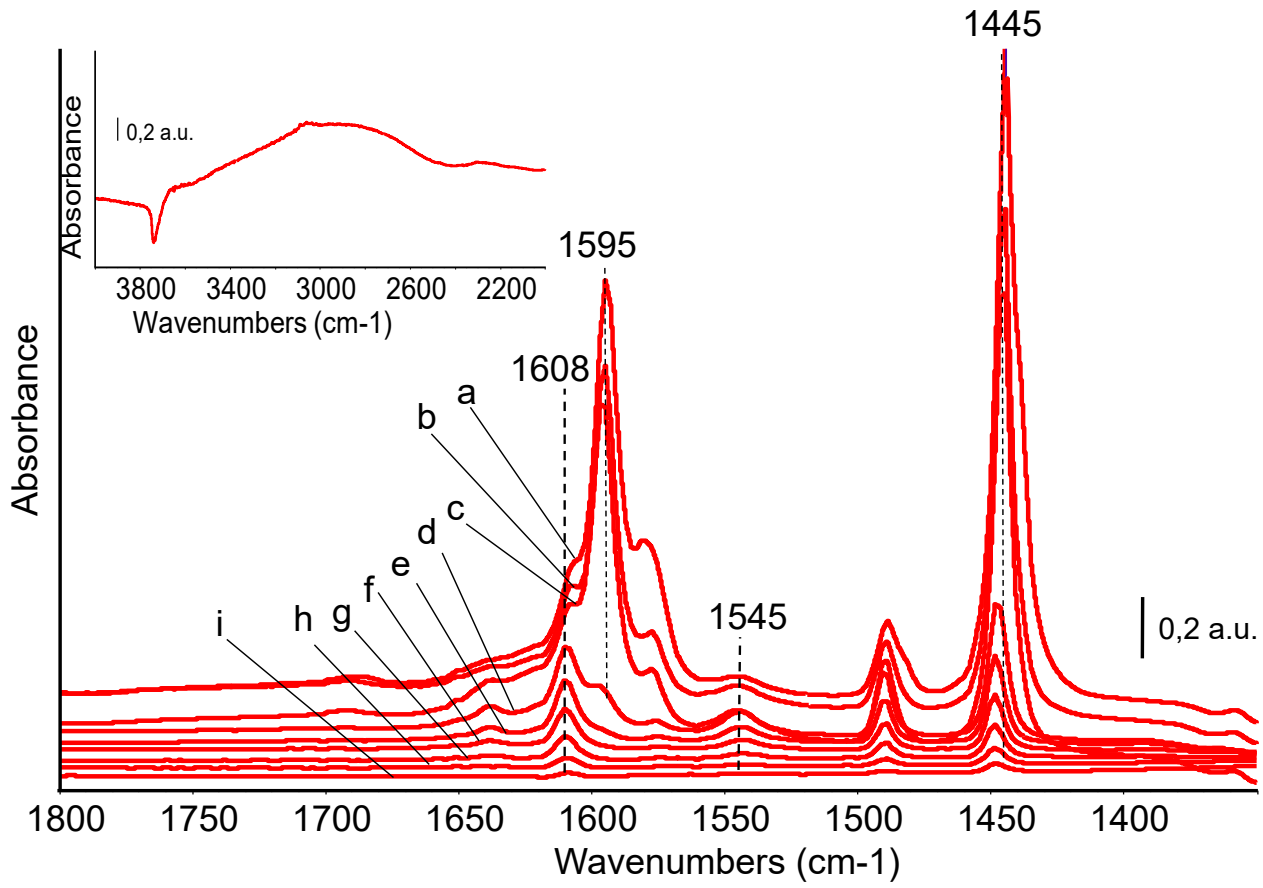

Figure 4. FT-IR subtraction spectra of adsorbed surface species arising from pyridine adsorption at room temperature over 5Nb2.5PSi sample (a) and after outgassing at room temperature (b), prolonged outgassing (40 min ca) at room temperature (c and inset, OH stretching region), outgassing at 423 K (d), 473 K (e), 523 K (f), 573 K (g), 623 K (h), 673 K (i). The activated surface spectrum has been subtracted.

The comparison of Fig. 4 with spectra reported in Fig. 3 shows that the shoulder above 1600 cm^{-1} assigned to pyridine coordinated over Lewis sites is already more evident in the spectrum of sample 5Nb2.5PSi recorded after outgassing at room temperature, in agreement with the highest Nb load over this catalyst. Indeed, this band becomes sharper and clearly centered at 1608 cm^{-1} after outgassing at increasing temperature. For both catalysts, OH bands described above appear as negative features in the subtraction spectra (insets in Figs. 3 and 4), consistent with the interaction of different families of hydroxyls with pyridine molecules (H-bonding and protonation).

In another set of experiments, 5Nb2.5PSi catalyst has been pretreated with 10 torr of water vapor for 20 minutes at room temperature directly in the IR cell and outgassed at room temperature for 5 minutes before pyridine adsorption. In fact, according to authors adsorbed water can generate Brønsted acidity on solid surfaces [29], and, otherwise, water can be

present in reaction media modifying the surface acidity of the catalysts. In particular, water is a product of the ethanol conversion reaction investigated here. After water vapor adsorption a broad band is detected in the range 3650-2800 cm^{-1} due to OH stretching mode of molecularly adsorbed water interacting with the surface hydroxyl groups through H-bonds. The corresponding deformation mode is detected as sharp and strong band at 1632 cm^{-1} (Fig. S5). A short outgassing (5 minutes ca) leads to the decrease in intensity of these features whereas the band assigned to isolated silanol is already partially restored at 3740 cm^{-1} pointing out the partial desorption of molecular water. Interestingly, no evidence of protonated water is observed [30], in agreement with the lower basicity of water with respect to pyridine, that is instead partly protonated. Over such “wet” surface, pyridine adsorption has been performed at room temperature, followed by desorption at increasing temperature, as described in the previous experiments (Fig. 5 for sample 5Nb2.5PSi). The spectrum recorded after pyridine adsorption and outgassing at room temperature shows the main bands previously discussed for molecular and protonated pyridine adsorbed over the dry surface, i.e. the peaks at 1596, 1546, 1490 and 1445 cm^{-1}. A broad and ill-defined adsorption centered at 1622 cm^{-1} is due to molecularly adsorbed water overlapped with the component near 1640 cm^{-1} due to pyridinium ions. A shoulder at 1608 cm^{-1} is still detectable, pointing out that pyridine coordinates over exposed Lewis sites even after pretreatment in water, in agreement with previous results reported on pyridine adsorption from aqueous phase over Nb-P-Si ternary oxide [16] and on hydrated Nb_2O_5 heterogeneous catalysts [31], as well as on other acidic oxides as alumina and silica-alumina [32].

This effect is not surprising considering that indeed pyridine is a stronger base than water, thus displacing water molecules from Lewis sites. Features of pyridine over Lewis sites become more evident following prolonged outgassing and, finally, the spectrum recorded at 423 K is completely consistent with the corresponding spectrum recorded over the dry catalyst surface. Although a direct quantification of acidic sites cannot be obtained from the IR data as reported, at 423 K the B/L ratio (ratio of number of Brønsted and Lewis sites), evaluated as [Intensity of the band at 1546 cm^{-1}/Intensity of the band at 1608 cm^{-1}], increases on the wet surface in comparison to the dry surface, and this could be due to an increased relative abundance of Brønsted sites, due to some dissociative adsorption of water.

Once again, the high frequency region of the subtraction spectra shows negative and complex band due to silanol species that interact with pyridine. Moreover, by subtracting the spectrum of the wet surface (i.e. the highly hydroxylated surface) from the spectrum after

pyridine adsorption we have the evidence of the complexity of the OH groups, showing several components at 3730, 3700 and 3640 cm^{-1} (Fig. S6), which, according to previous literature [20,21,22], could be due to Si-OH, Nb-OH and P-OH groups, respectively.

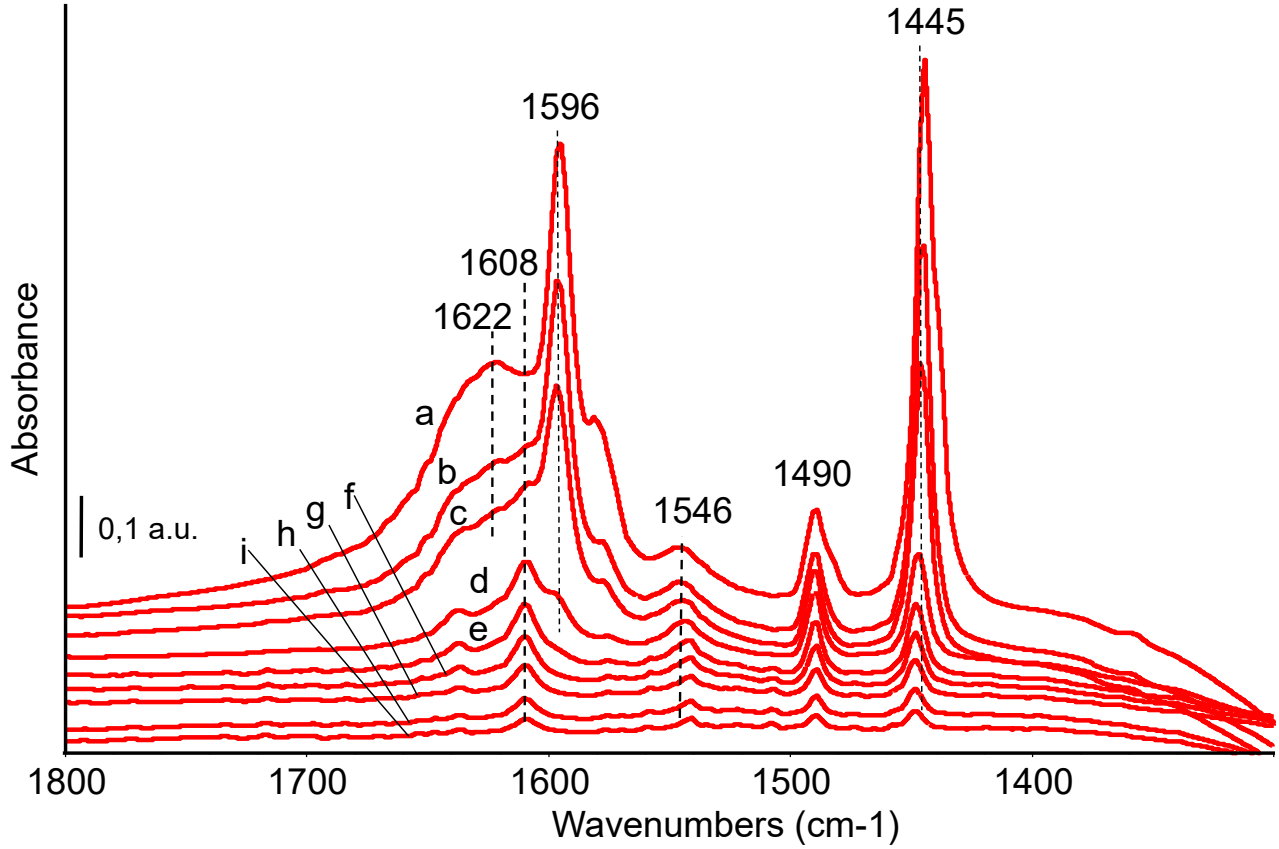

Figure 5. FT IR subtraction spectra of adsorbed surface species arising from pyridine adsorption at room temperature over wet 5Nb2.5PSi sample (a) and after outgassing at room temperature (b), prolonged outgassing at room temperature (40 min ca) (c), outgassing 423 K (d), 473 K (e), 523 K (f), 573 K (g), 623 K (h), 673 K (i). The activated surface spectrum has been subtracted.

Samples acidity was studied quantitatively carrying out acid-base titrations by using ammonia as a basic probe in the gas phase, and 2-phenylethylamine (PEA) in the liquid phase. The two probes are both highly basic, but they have different kinetic diameters. NH_3 is a very small molecule with a kinetic diameter of 2.6 Å, that allows entering into almost all the micropores of 2.5Nb2.5PSi and 5Nb2.5PSi and thus probing the acid sites present at both internal and external surfaces. Conversely, the larger PEA molecule, with dimensions of approximately 7 Å, may not have access to the exposed acid sites on the inner surface of micropores. Therefore, the comparison of the titration results with NH_3 and PEA probes could provide valuable information on the accessibility of acid sites in the two samples. Ammonia titration was carried out under gas-solid phase, while PEA titration under liquid-

solid phase, by using an apolar and aprotic solvent, cyclohexane, to have an inert environment.

The adsorbed amounts of NH_3 and PEA calculated from the collected adsorption isotherms are reported in Table 2, expressed as acid site number (μmol g^{-1}) and acid site density (μmol m^{-2}).

Table 2. Surface acid sites of the Nb-P-Si samples measured with NH_3 (for gas-solid phase titration) and PEA (for liquid-solid phase titration) probes.

Sample	NH_3 Probe (gas-solid) [17]		PEA Probe (liquid-solid)	
	Acid site number μmol g^{-1}	*Acid site density* μmol m^{-2}	*Acid site number* μmol g^{-1}	*Acid site density* μmol m^{-2}
2.5Nb2.5PSi	463.35 ± 22.11	1.14 ± 0.12	234 ± 8 (91%) [a]	0.58 ± 0.08
5Nb2.5PSi	536.96 ± 6.01	1.48 ± 0.15	457± 15 (37%) [a]	1.25 ± 0.17

[a] Strong acid sites, in percent.

Regarding gas-solid phase NH_3 titration, 5Nb2.5PSi adsorbs a slightly larger amount (537 μmol g^{-1}) of basic probe than 2.5Nb2.5PSi (463 μmol g^{-1}). This difference may be expected because it reflects the different composition of the two materials; indeed, the higher the Nb content (5Nb2.5PSi), the more abundant the acid sites are, as expected in relation to the Lewis and Brønsted acidity provided by niobium centres. It is interesting to note that 5Nb2.5PSi showed more acid character than 2.5Nb2.5PSi even if it possesses lower surface area (Table 1), thus showing also a higher acid site density. In fact, the surface of the silica component does not provide Lewis acidity nor Brønsted acidity sufficiently strong to protonate ammonia [24].

Liquid–solid PEA adsorption isotherms are reported in Fig. 6. The obtained curves show asymptotic profiles, which are well fitted by Langmuir model. The total number of sites reported in Table 2 (234 μmol g^{-1} and 457 μmol g^{-1} for 2.5Nb2.5PSi and 5Nb2.5PSi, respectively) was computed from the first isotherm collected at 303.0 K (assuming a 1:1 stoichiometry for the PEA adsorption on the acid site). After solvent flowing and cleaning, a second adsorption was realized; from the difference between the number of PEA adsorbed moles in the first and second runs, the so called “irreversibly” adsorbed amount of PEA was computed with the possibility to evaluate strong acid sites of the samples.

In the case of 2.5Nb2.5PSi, the acidity probed by PEA (234 μmol g^{-1}) is almost 50% of the total acidity measured using ammonia (463 μmol g^{-1}), while only a slight decrease is observed for 5Nb2.5PSi, comparing the NH_3 (537 μmol g^{-1}) and PEA (457 μmol g^{-1}) titrations. These outcomes agree with morphological analysis (Table 1), showing that the

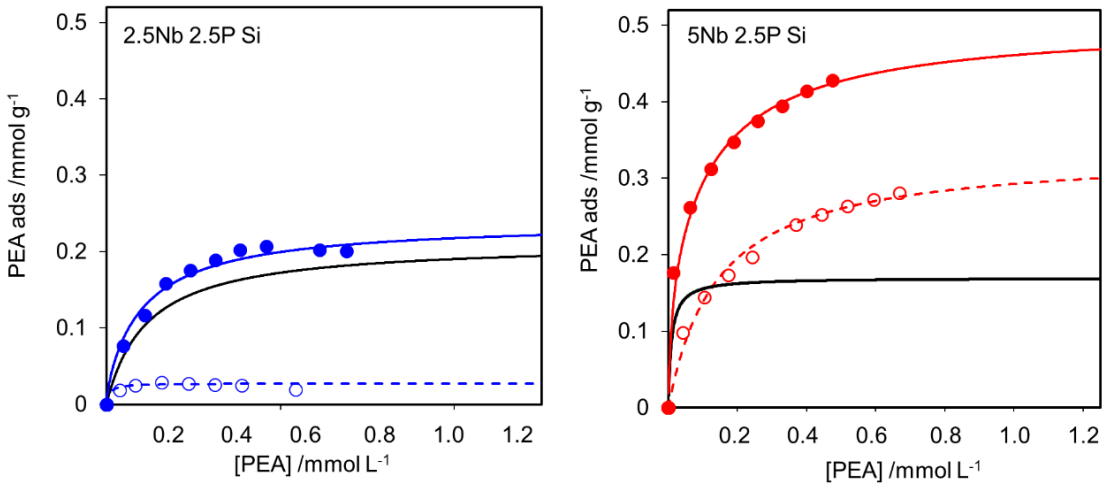

Figure 6. Adsorption isotherms of PEA probes at 303 K on 2.5Nb2.5PSi (left panel) and 5Nb2.5PSi (right panel) samples evaluated in cyclohexane, for determining the *intrinsic* acidity. Full markers and empty markers represent the I° and the II° run adsorptions, respectively. Black lines represent the calculated Langmuir curves of PEA adsorptions on strong acid sites; (blue and red) dotted lines represent the calculated Langmuir curves of the II° (reversible adsorption) runs; blue and red lines represent the total (reversible plus irreversible) adsorption trends of the I° runs, obtained as sum of the dotted and the black solid lines.

accessibility of acid sites is lower in 2.5Nb2.5PSi, which possesses smaller micropores than 5Nb2.5PSi.

Concerning the number of strong acid sites, almost the totality (91%, corresponding to ca. 213 μmol g^{-1}) of acid sites probed by PEA are strong sites in 2.5Nb2.5PSi, whereas strong sites account for only 37% of acid sites titrated in 5Nb2.5PSi (169 μmol g^{-1}). Likely, the higher Nb-concentration in 5Nb2.5PSi results mainly in a higher number of weaker Brønsted/Lewis sites at the surface.

The presence of a larger amount of strong sites in 2.5Nb2.5PSi than in 5Nb2.5PSi was confirmed by NH_3-TPD experiments (Fig. 7), which revealed that NH_3 desorbed from 2.5Nb2.5PSi and 5Nb2.5PSi surfaces with comparable strength (T_{max} was observed at *ca.* 618 K in any case), but in different amount (430 μmol g^{-1} and 367 μmol g^{-1} for 2.5Nb2.5PSi and 5Nb2.5PSi, respectively).

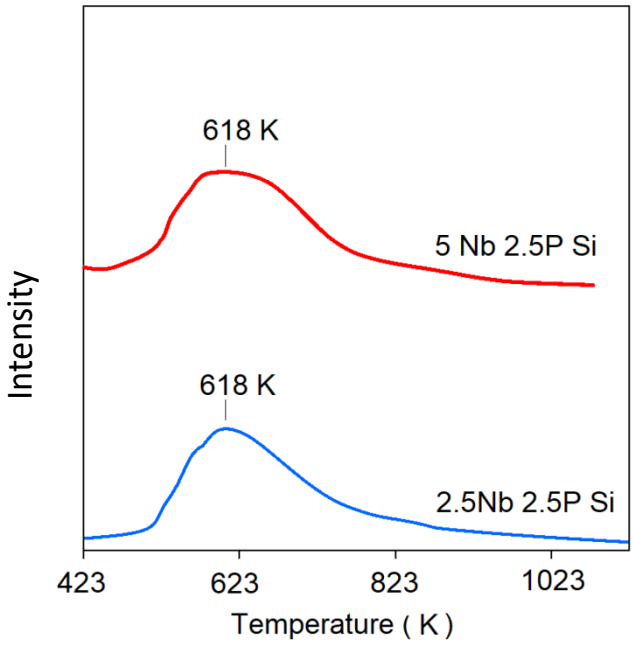

Figure 7. NH_3-TPD profiles as a function of temperature of 2.5Nb2.5PSi (blue) and 5Nb2.5PSi (red) calcined (773 K), collected as described in Experimental section. Both 2.5Nb2.5PSi and 5Nb2.5PSi samples showed the same value of T_{max} (*ca*. 618 K). The amount of desorbed ammonia was 430.5 μmol g^{-1} for 2.5Nb2.5PSi and 367.2 μmol g^{-1} for 5Nb2.5PSi.

3.3 Catalytic conversion of ethanol in Temperature Programmed Surface Reaction conditions.

In Fig. 8 the results of ethanol TPSR with 1 % ethanol feed are reported. In both cases, the light-off temperature for ethanol conversion is found at ~ 550 K, with ethylene as the only

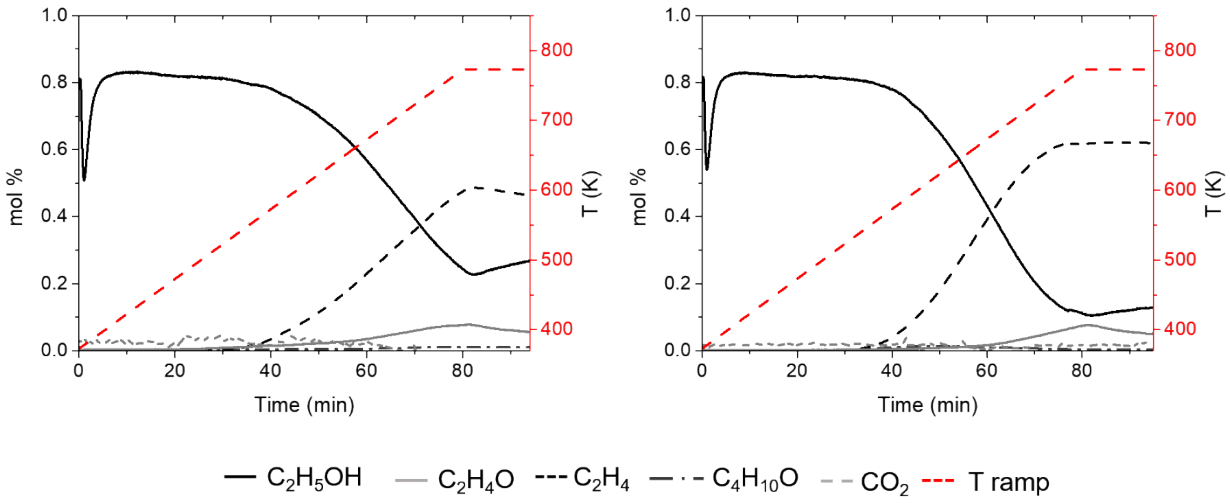

Figure 8. Ethanol TPSR experiments with 1% Ethanol feed: 2.5Nb2.5PSi left, 5Nb2.5PSi right.

product, followed by acetaldehyde production with light-off at ~ 650 K. Thus, the following reactions are observed to occur:

$CH_3CH_2OH \rightarrow H_2C=CH_2 + H_2O$ (1)

$CH_3CH_2OH \rightarrow CH_3CHO + H_2$ (2)

i.e. monomolecular dehydration and dehydrogenation, respectively. With both catalysts, in the last part of the experiment the temperature increase was stopped at 773 K and a dwelling step at constant temperature was realized. At 773 K ethanol conversion is 76% and 87 % over 2.5Nb2.5PSi and 5Nb2.5PSi, respectively, suggesting that additional niobium results in increased reaction rate, likely due to increased acid density. This agrees with the above data. In fact, the dehydration reactions do not need strong acidity, thus the more abundant acidity of 5Nb2.5PSi, despite being constituted by relatively weak sites (see above), allows higher catalytic activity than 2.5Nb2.5PSi. Upon the dwelling step, ethanol conversion and both ethylene and acetaldehyde yields were decreasing with time over 2.5Nb2.5PSi catalyst, suggesting that active sites for both reactions undergo partial deactivation. In contrast, over the 5Nb2.5PSi catalyst only acetaldehyde yield decreases with time in the dwelling time, ethylene yields being nearly constant. In any case, no other products, including di-ethyl-ether and ethyl-acetate, were observed in these experiments. Thus, ethylene selectivity is essentially 100% at low conversion in the 550-650 K range over both catalysts. Ethylene selectivity decreases to 87 %, with 13 % selectivity to acetaldehyde, at 773 K over 2.5Nb2.5PSi, while over 5Nb2.5PSi the selectivities to ethylene and acetaldehyde at 773 K are 89% and 11%, respectively.

The same experiment has been repeated using a higher ethanol partial pressure, with 2.5 % ethanol / nitrogen feed, whose results are reported in Fig. 9.

The curve observed on 2.5Nb2.5PSi is similar to the previous one although the conversion of ethanol is lower at each temperature and product selectivity ratio is slightly shifted towards acetaldehyde (77% ethylene; 23 % acetaldehyde at 773 K). In contrast, the increase in ethanol feed molar fraction produces a more important variation on the product distribution over the 5Nb2.5PSi catalyst; in this case, acetaldehyde starts to be produced already at 500 K, achieving a maximum at 773 K with a selectivity as high as 33 mol.% (ethylene selectivity 67%).

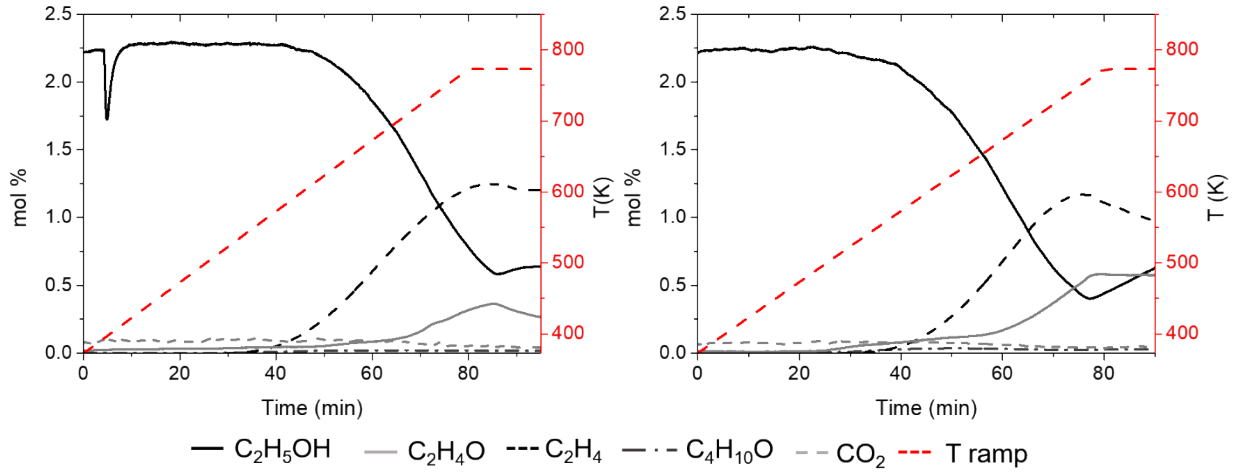

Figure 9. Ethanol TPSR experiments with 2.5 % Ethanol feed: 2.5Nb2.5PSi left, 5Nb2.5PSi right.

This suggests that the additional niobium sites in 5Nb2.5PSi catalyst are more active in dehydrogenation reaction (2) than those present in 2.5Nb2.5PSi catalyst. Again, diethyl ether and ethyl-acetate are not observed in significant quantities. Interestingly, using alumina catalysts in the same conditions diethylether is produced in significant amounts and starts to be produced before ethylene, as reported previously [33]. Indeed, diethylether is commonly produced over all catalysts at low ethanol conversion and low temperatures, while ethylene is produced at higher temperatures and ethanol conversion [34,35,36,37]. Indeed the industrial manufacture of diethylether is realized over alumina catalysts at partial ethanol conversion [38,39].

Taken into consideration the slight deactivation phenomenon observed in the dwelling step in previous experiments (which may have several different origins), and the production of acetaldehyde (that can occur via pure dehydrogenation but also by oxidative dehydrogenation), experiments have been carried out in oxidizing conditions too. The oxygen feed content chosen is in principle sufficient to allow full ethanol combustion. Experiments in oxidative conditions were carried out at the same ethanol molar fraction chosen for the non-oxidative ethanol TPSR experiments in order to evaluate the effect of oxygen in the same fluido-dynamic conditions (Fig. 10). Oxygen introduction is not affecting the light-off temperatures for ethanol conversion, ethylene and acetaldehyde production (with a very small increase in acetaldehyde selectivity) but it only shows a prominent effect in the increase of the acetaldehyde content at temperatures above 600 K, and stabilizing its yield in the dwelling step.

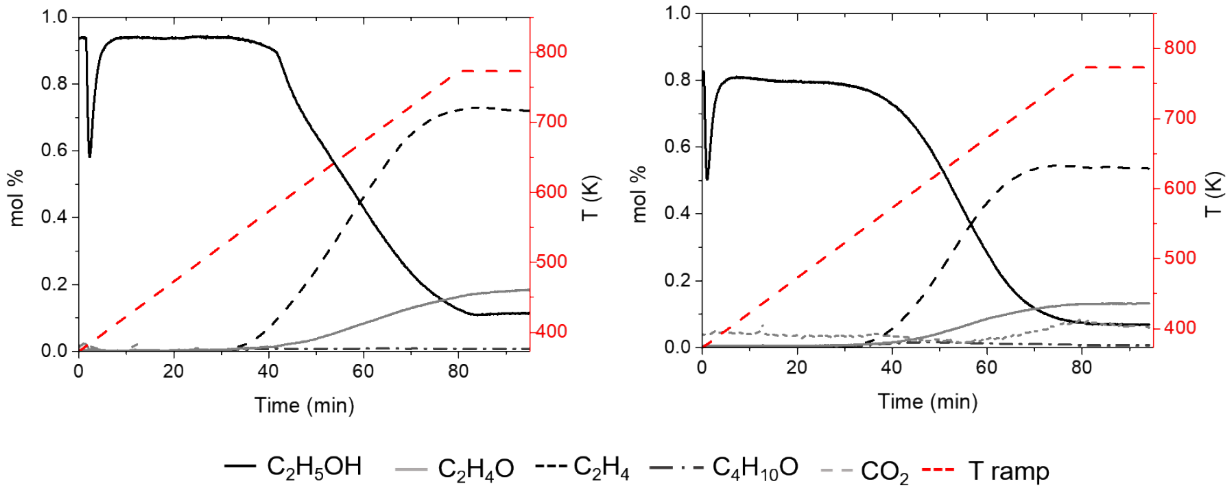

Figure 10. Oxidative Ethanol TPSR experiments, with 1% EtOH/ 6% O_2/ 93% N_2: 2.5Nb2.5PSi left, 5Nb2.5PSi right.

For the higher Nb loading, also CO_2 appears at high temperature among reaction products, certainly coming from ethanol total oxidation. These data suggest that the presence of oxygen does not affect the dehydration and the (pure) dehydrogenation reactions to ethylene and acetaldehyde, while stopping the deactivation effect in the dwelling step. This effect can be due to limiting niobium reduction to lower oxidation states and (at least for 5Nb2.5PSi catalyst) burning carbonaceous material deposited on the surface.

3.4 Catalytic conversion of ethanol in Steady State conditions

In Fig. 11, the results for steady state experiments are reported. They have been realized in the presence of oxygen, taking into consideration the limited effect of oxygen on product selectivity and the positive effect in limiting deactivation. The results are in good agreement with those obtained in transient conditions, showing that ethylene is main product for the whole T range. 5Nb2.5PSi is more active than 2.5Nb2.5PSi at 623 and 673 K in ethylene production and, for this catalyst, no temperature effect is observed above 723 K, suggesting possible diffusion limitation or a change in the catalyst structure. The best ethylene yields are obtained at 773 K over the 5Nb2.5PSi catalyst, at 88 mol% ethanol conversion, 83 mol% selectivity to ethylene, and 11 % selectivity to acetaldehyde and 6 % to CO_2. Over the 2.5Nb2.5PSi catalyst conversion is definitely lower as well as ethylene selectivity. Also in these conditions, the production of diethylether and ethylacetate is near zero.

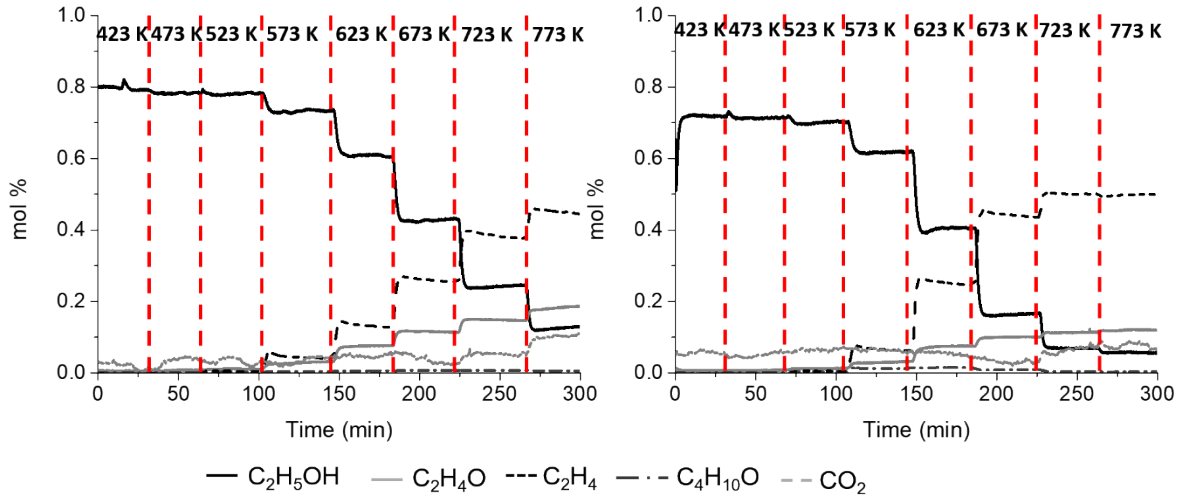

Figure 11. Results of steady state experiments: 2.5Nb2.5PSi left, 5Nb2.5PSi right.

3.5 Study of the effect of contact time on catalytic conversion

The effect of contact time has been evaluated, by choosing two different ethanol feed molar fractions, and working at low ethanol conversion. In Figs. 12, 13 and 14, the obtained concentration profiles as a function of time and total flow rate are reported. These data confirm that 2.5Nb2.5PSi is less active than 5Nb2.5PSi, even though both show an almost total selectivity towards ethylene in such low conversion conditions. However, small amounts of dethylether are observed at low flow rate, but decreases almost to zero at higher flow rate. This suggests that diethylether is a secondary product, while ethylene is the primary product. Thus, diethylether should not form as usual by dehydration of ethanol,

$$2\ CH_3CH_2OH \rightleftharpoons (CH_3CH_2)_2O + H_2O \qquad (3)$$

occurring [40,41] at lower temperature and conversion than dehydration to ethylene (reaction (1), but from addition of ethanol to ethylene

$$CH_3CH_2OH + H_2C{=}CH_2 \rightleftharpoons (CH_3CH_2)_2O \qquad (4)$$

As expected, at lower flow rates, i.e. higher contact times, the conversion of ethanol is markedly higher than at higher flow rates. On the other hand, the effect of contact time is more pronounced in the case of the more active catalyst (5Nb2.5PSi) and with the lower ethanol concentration. Indeed, ethanol conversion is higher at lower ethanol feed concentration, suggesting that a self-inhibition occurs, leading to a negative reaction order of ethanol in the production of ethylene. The effect of contact time is far less evident at lower reaction temperatures, where conversion is very low (Fig. 14).

Catalysts deactivation is more remarkable at the lower Nb loading, possibly due to the higher density of very strong acid sites, and at lower flow rate.

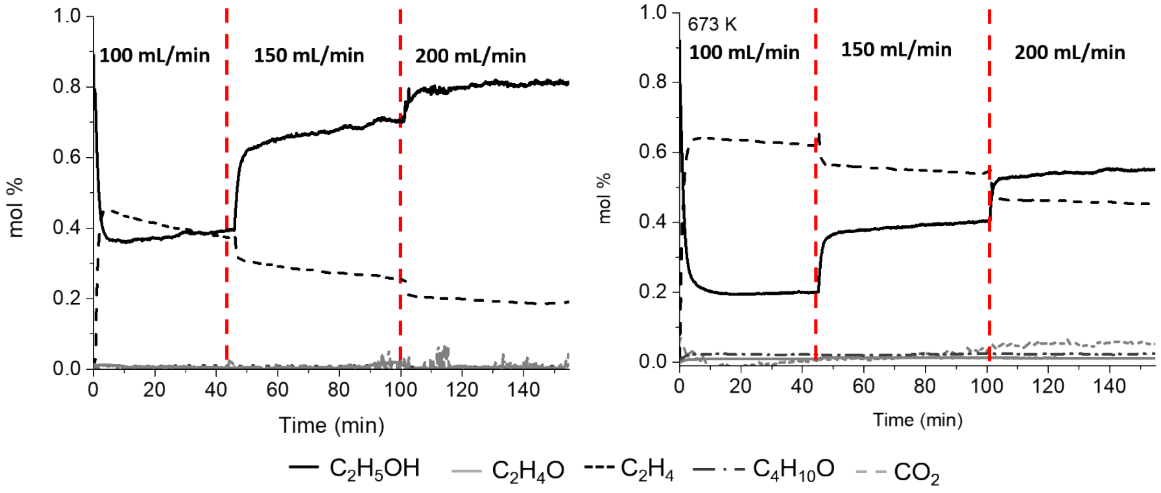

Figure 12. 2.5Nb2.5PSi left, 5Nb2.5PSi right, 1% EtOH at 673 K.

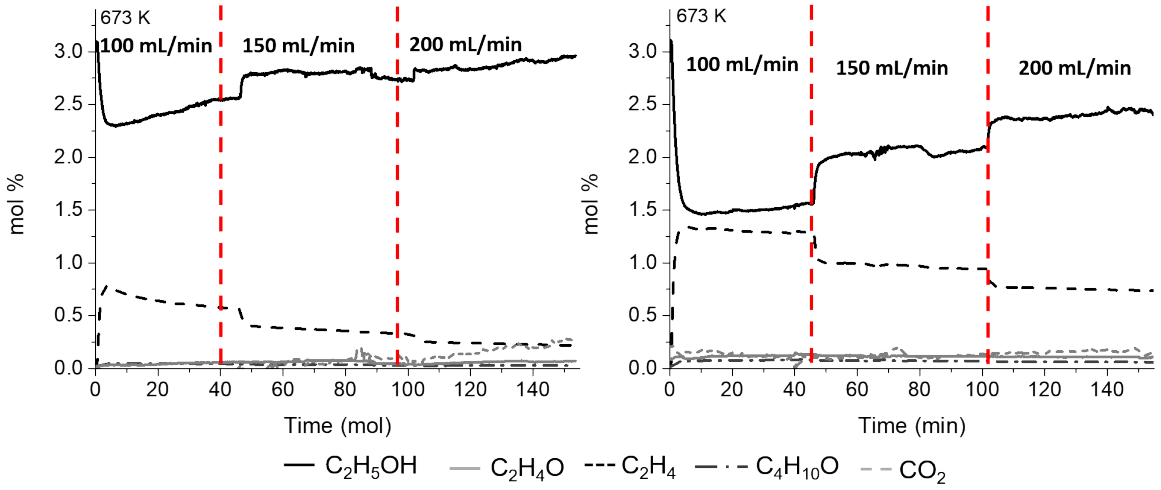

Figure 13. 2.5Nb2.5PSi left, 5Nb2.5PSi right, 3% EtOH at 673 K.

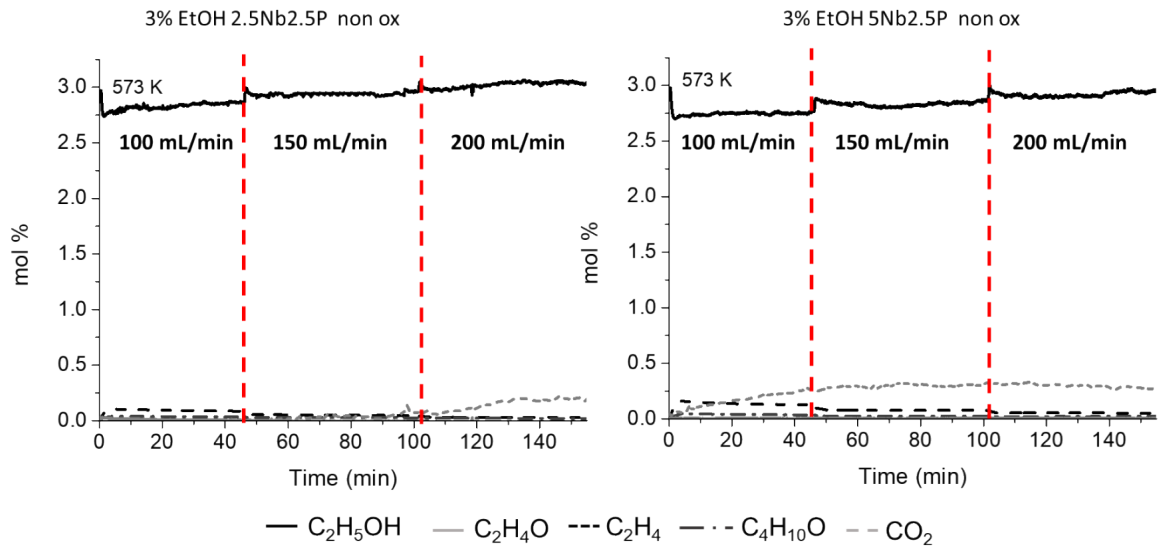

Figure 14. 2.5Nb2.5PSi left, 5Nb2.5PSi right, 3% EtOH at 573 K.

3.6 Evaluation of the apparent activation energy and reaction order for the ethanol dehydration to ethylene

From the catalytic data obtained at low conversion, and in absence of other products in that regime (in particular only traces of diethylether) it is possible to evaluate the kinetic parameters of reaction (1) over these catalysts. The apparent activation energy can be evaluated from the conversion data at different temperatures: the obtained values are 111 kJ/mol and 133 kJ//mol for 2.5Nb2.5Psi and 5Nb2.5Psi, respectively. These data are compared with difficulty with literature data, because over most catalysts the dehydration reaction to diethylether (reaction 3) is far faster than that to ethylene (reaction 1) at low temperature: this makes difficult the evaluation of the activation energy of reaction 1 at low temperature and conversion. However, it can be compared with values calculated for the reaction (1) supposed to be realized in the protonic acid H-MOR zeolite: in this case very small value 146.0 and 177.2 kJ/mol are reported for two different mechanisms [42]. In any case these apparent activation energy data indicate that our experiments are realized under chemical kinetic control, as they do also in the case of the experiments realized in oxidizing atmospheres, where apparent activation energy values around 90 kJ/mol are measured for ethanol conversion.

From the conversion data using different feed concentrations, the reaction order measured in steady state conditions is in the range 0.1-0.5 for both catalysts at 673 K. Such a slightly positive reaction order confirms that ethanol adsorption is very strong and that active sites are almost saturated in these conditions.

3.7 In-situ FT-IR study of ethanol adsorption and conversion.

Ethanol adsorption and thermal evolution at the catalyst surfaces, as well as the parallel formation of gas phase species, have also been also investigated as a function of the temperature in static conditions in an IR cell using a catalyst pressed disk (range 423K-673 K). Results of the corresponding blank experiment (i.e. ethanol thermal evolution in the empty IR cell) are reported in figure S7 evidencing no reactivity in the same temperature range.

In Fig.15 (top panel), the surface species spectra recorded after ethanol adsorption over sample 2.5Nb2.5PSi show the typical bands of CH deformation modes centered at 1482, 1450, 1397, 1383 sh, 1358 cm^{-1}. The corresponding CH stretching modes at 2981, 2940 split, 2910, and 2885 cm^{-1} are reported in in the inset [31].

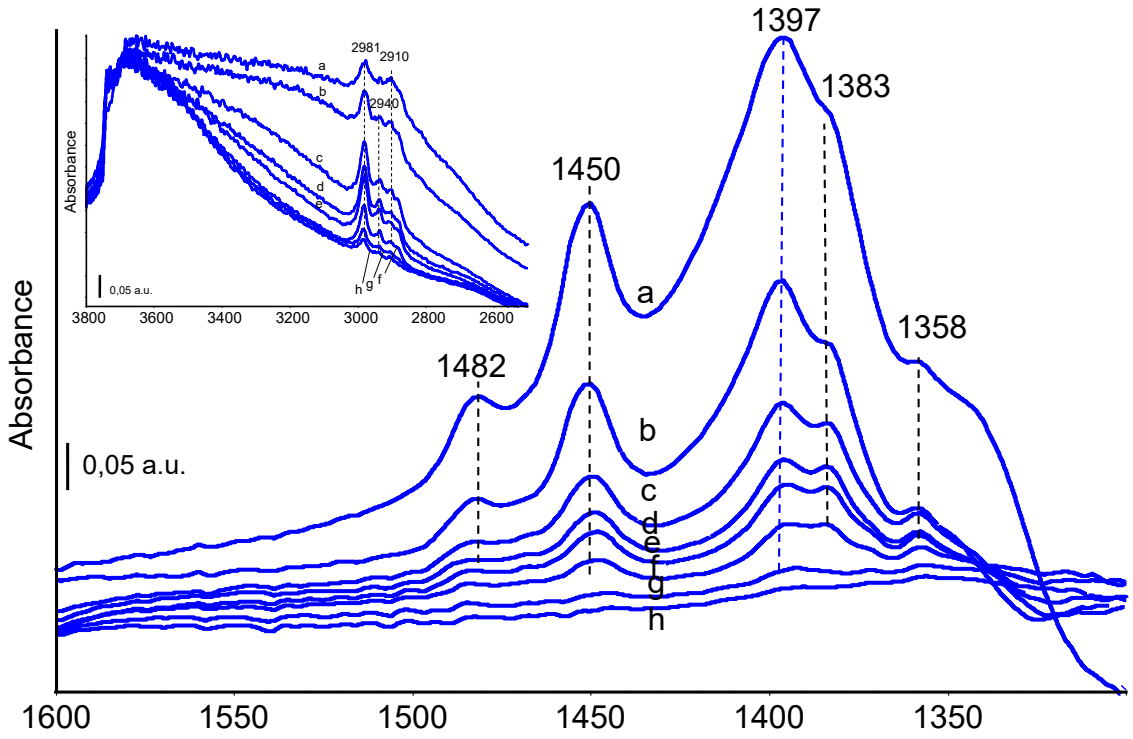

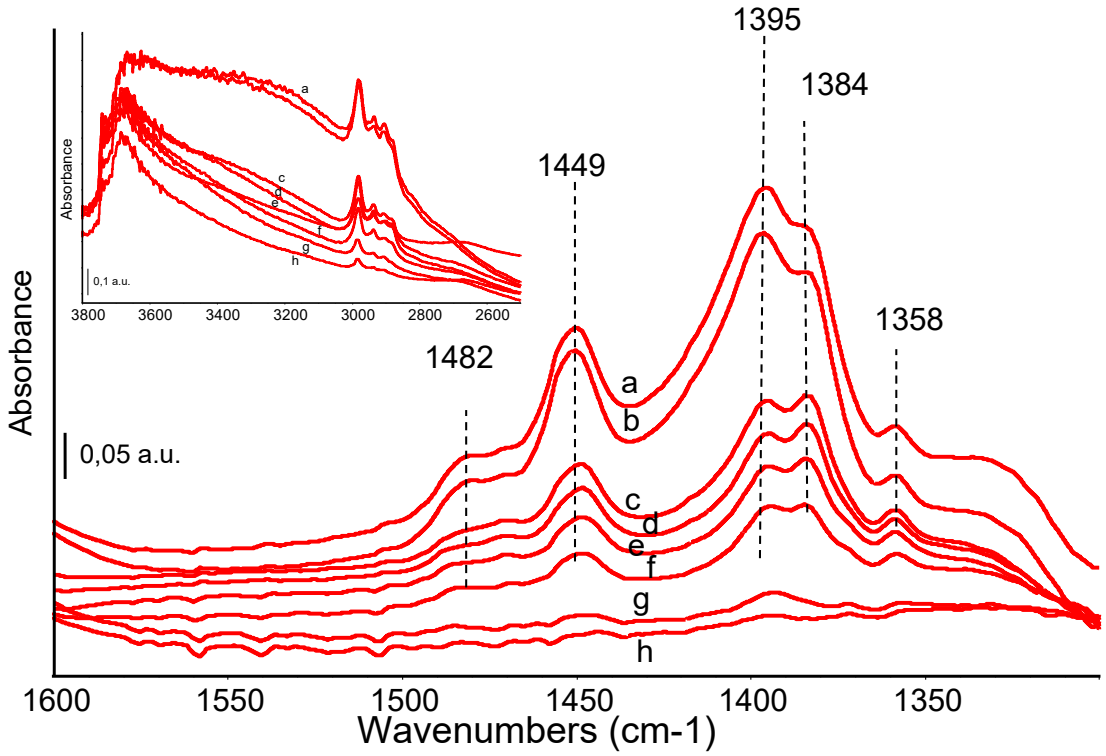

Figure 15. FT-IR subtraction spectra of surface species arising from ethanol adsorption and thermal evolution over sample 2.5Nb2.5PSi (top) and 5Nb2.5PSi (bottom), in ethanol at room temperature (a), after short outgassing at room temperature (b), 423 K (c), 473 K (d), 523 K (e), 573 K (f), 623 K (g), 673 K (h). The activated surface spectrum has been subtracted. In the inserts: unsubtracted spectra in the OH and CH stretching region.

CH stretching and deformation bands are detected almost unchanged in shape and position and progressively decreasing in intensity in the overall temperature range up to 573 K, while at 623 K they essentially disappear. A small change in relative intensities can be detected for the split band in the range 1390-1370 cm^{-1}. This band is assigned to symmetric bending modes of the CH_3 group and its splitting could be due to the formation of different adsorbed species. In the inserts, the behavior of OH stretching bands can be observed. While the complex absorptions in the 3800-3500 cm^{-1} region are due to surface hydroxy groups of the catalysts, as discussed above, the very broad absorption centered around 3200 cm^{-1} is likely due to the OH stretching mode of adsorbed undissociated ethanol. This absorption is essentially disappeared at 473 K, suggesting that at this temperature the residual bands are due to adsorbed ethoxy-groups. No information can be obtained by the analysis of the low frequency region, i.e. the CO/CC stretching region, masked by the strong absorptions of the silica lattice.

The splitting of the CH_3 bending mode and the different behavior of the two components under outgassing and at increasing temperatures suggests that they are due to two different

types of ethoxy groups, e.g. bonded to silica and to Nb and/or P atoms, i.e. weakly adsorbed and strongly adsorbed). Negative bands in the OH stretching region appearing in the subtraction spectra at room temperature (figure S8 in Supporting Information) provide evidence of the first interaction of ethanol or ethoxy groups with the hydroxyl groups. A very similar behavior characterizes ethanol adsorption and conversion over the 5Nb2.5PSi system (Fig. 15, bottom panel).

In Fig. 16 gas phase spectra recorded at increasing temperatures within the same experiment are reported and exemplified for sample 5Nb2.5PSi. In the gas phase spectra bands of residual and desorbed ethanol vapor (EtOH) are detected up to 573 K. ~~Starting from this temperature, n~~New features appear in the spectrum recorded at 523 K: a rotovibrational band at 950 cm^{-1} (PQR profile, $=CH_2$ wagging mode) assigned to ethylene and a weak band at 1135 cm^{-1} assigned to diethylether DEE (CO stretching mode) [41].

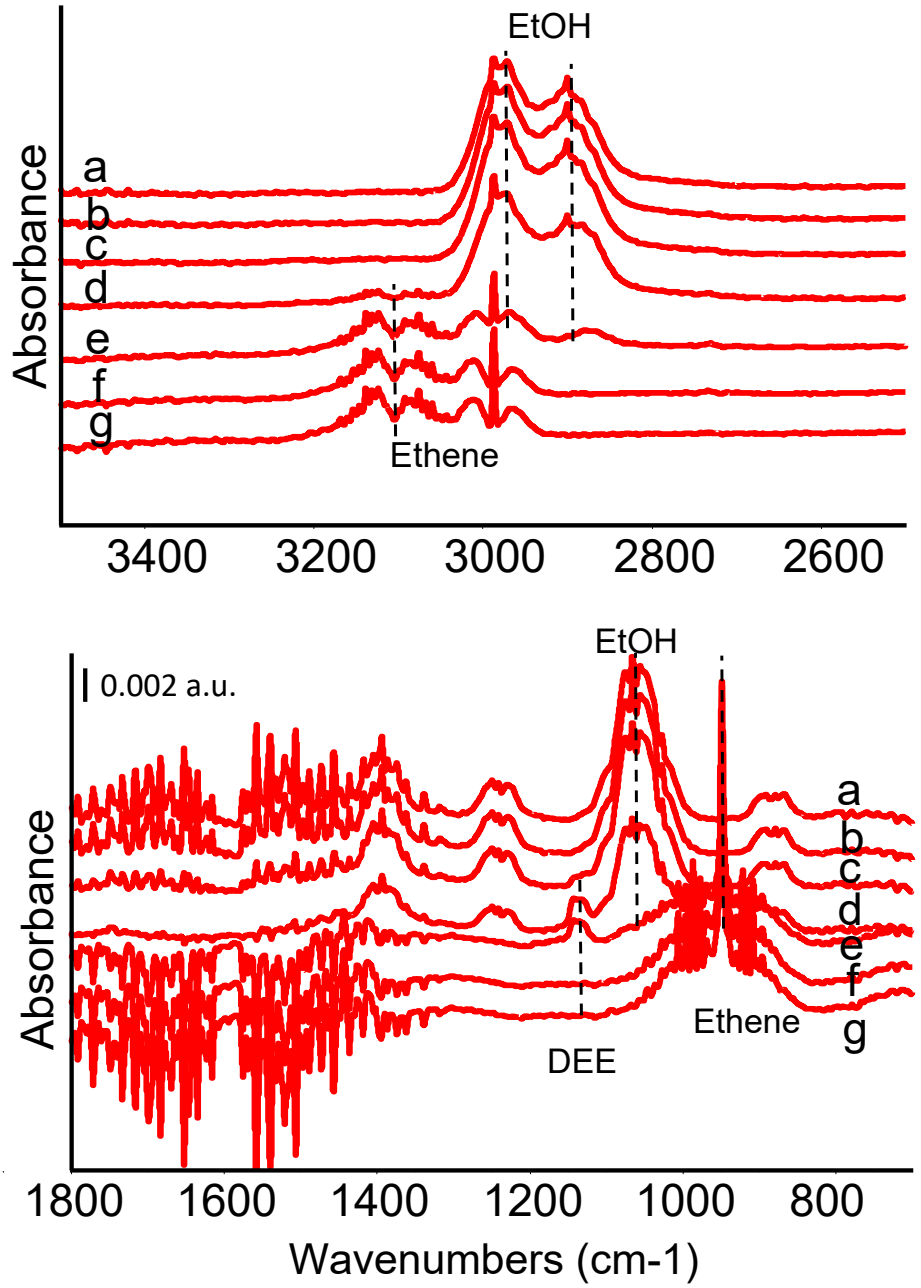

Figure 16. Gas phase species arising from ethanol thermal evolution over catalyst 5Nb2.5PSi at 423 K (a), 473 K (b), 523 K (c), 573 K (d), 623 K (e), 673 K (f), 723 K (g). Top panel: high frequency region.

At 573 K other bands can be clearly detected, consistent with the formation of ethylene (2990 cm^{-1}, CH stretching mode, 3108 cm^{-1}, $=CH_2$ stretching mode) and ether (2870 cm^{-1}, CH stretching mode, and 1100 cm^{-1}, C-O stretching mode). Spectra of ethanol conversion over 2.5Nb2.5PSi catalyst are also reported in figure S9.

Comparing band intensities, on both catalysts diethylether is already detected in traces at 523 K and peaks at 573 K, whereas ethylene starts to be detected in traces at 523 K and its

amount still increases up to 673 K. Almost complete ethanol conversion is observed above 573 K.

It is relevant to remark that, while diethylether is almost not observed in catalytic experiments, also at very low ethanol conversion, small amounts of it are observed in the spectroscopic experiments. It is however to be noted that also this experiment, compared with those realized with other catalysts [**Error! Bookmark not defined.**,**Error! Bookmark not defined.**], reveal the very weak activity of these catalysts in producing diethylether. On the other hand, diethylether does not appear at lower temperature than ethylene (as found on most catalysts) but at the same temperature as ethylene. Thus, this result can be taken as a confirmation that diethylether over these catalysts does not form by ethanol dehydration reaction (3) but by ethanol addition to ethylene, reaction (4), as supposed above on the basis of steady state conversion experiments at different contact times.

The different behavior of these catalysts with respect to most of the ethanol dehydration catalysts reported in the literature may be associated to a substantial lack of strong acid-base sites on the surface of NbPSi catalysts (as reported for similar samples [15]), able to adsorb ethanol undissociatively. In fact, according to our previous studies [40], the most common mechanism for diethylether production likely implies the nucleophilic substitution of ethoxy groups on activated undissociated ethanol molecules adsorbed on acid-base sites. The small amounts of diethylether formed in the 523 – 623 K temperature range, possibly due to the reaction of ethylene with ethanol, is cracked back either by the inverse of the same reaction (4), more favored at higher temperatures, or by reaction

$(CH_3CH_2)_2O \rightarrow 2\ H_2C{=}CH_2 + H_2O$ (5)

occurring above 623 K.

To collect more information, in the same conditions, adsorption and thermal evolution of diethylether have been tested over the most active catalyst, 5Nb2.5PSi. IR spectra of adsorbed species and gas phase species are reported in Fig. 17. In the spectra of the catalyst surface, bands at 1450 and 1390 cm^{-1} are due to the asymmetric and symmetric CH deformation modes of the CH_3 group. CH_2 deformation modes are evident at 1470 and 1350 cm^{-1} (figure 17 top panel). Correspondingly, the CH stretching bands are detected in the high frequency region of the spectra at 2982, 2940, 2900 (sh) and 2884 cm^{-1} (Fig. S10). Above 523 K a very weak band can be observed just below 1700 cm^{-1} and likely assigned to traces of adsorbed carbonyl compounds such as acetaldehyde, together with some adsorbed water (inset in figure 17, top panel). The persistence of the band at 1350 cm^{-1}, which is not observed with adsorbed ethanol, suggests that the adsorbed species are

constituted mainly by intact diethylether. These features are progressively weakened following temperature evolution up to 623 K, but no changes in position can be detected. The analysis of gas phase spectra evidences ethylene formation between 523 and 573 K (Fig. 17 bottom panel) that further increases until complete diethylether conversion at 723 K. No other reaction products are detected in these conditions. This indicates that diethylether cracking occurs through reaction (5) more than through the inverse of reaction (4), taking into account that in the conditions reaction (1) is already occurring fast.

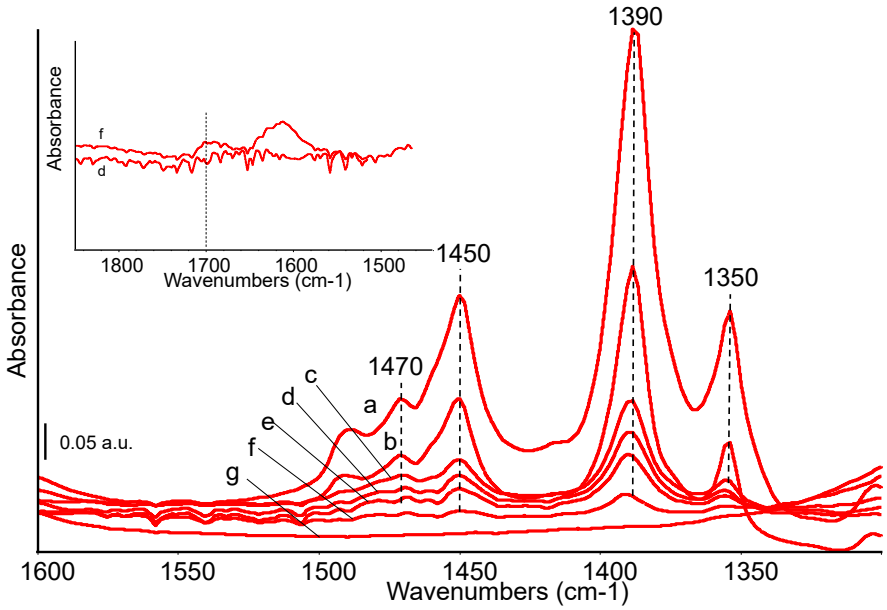

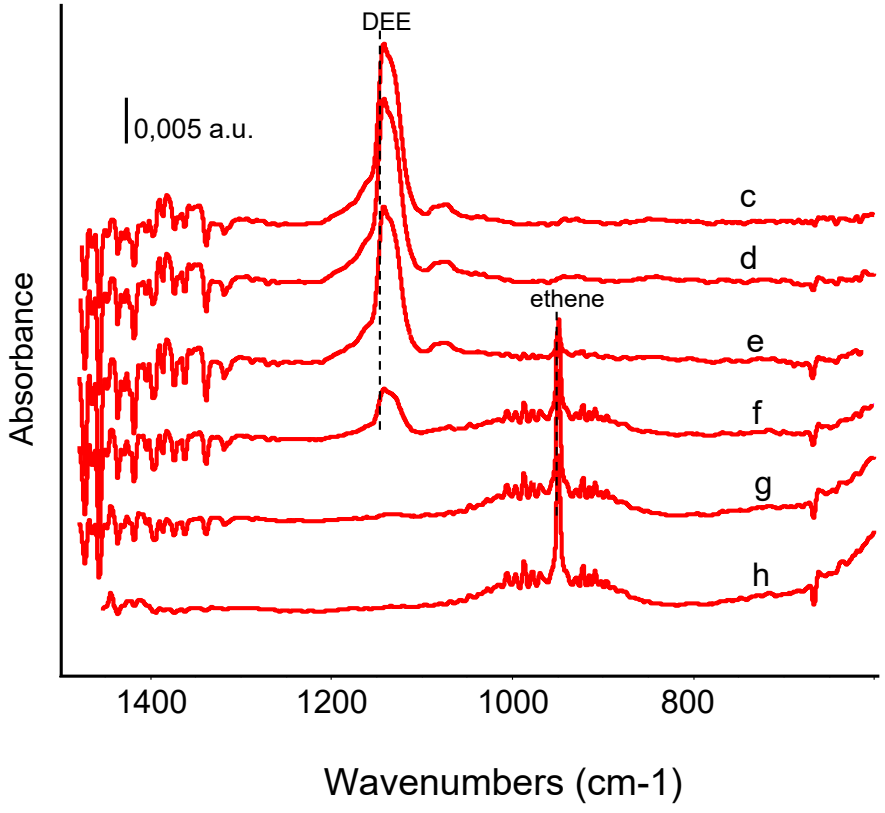

Figure 17. FT-IR subtraction spectra of surface species arising from DEE adsorption and thermal evolution over 5Nb2.5PSi catalyst (top panel) and corresponding gas phase species (bottom panel). In DEE at room temperature (a) and after short outgassing at room temperature (b), at 473 K (c), at 523 K (d), 573 K (e), 623 K (f), 673 K (g), 723 K (h). The activated surface spectrum has been subtracted from spectra in the top panel. Inset: detail of the vC=O region.

Pyridine adsorption has been carried out over the "spent" surface of 5Nb2.5PSi catalyst after reaction of ethanol in the IR cell and leads to spectra consistent with those reported in the previous paragraphs for the fresh sample (Fig. S11). The intensity ratio B/L signals (i.e. Brønsted to Lewis signal intensity ratio I_{1545}/I_{1610}) is slightly higher in the sample after ethanol conversion. New Brønsted sites might be formed also by hydration of the catalyst by produced water vapor during the reaction itself, but on the other hand Lewis sites can be poisoned by coke formation.

Conclusions

The results of this study show that gel-derived Nb_2O_5-P_2O_5-SiO_2 solids are effective acidic catalytic materials with high-surface area and a combination of mesoprosity and microporosity. The samples retain S_{BET} surface areas ~ 350 m^2/g after calcination at 773 K. IR experiments show the presence, on the surface in the vacuum/solid interface, of hydroxy groups typical of silica-based materials (silanol groups), but also P-OH and/or Nb-OH groups. IR studies of adsorption of pyridine in the gas/solid interface demonstrate that the samples show Brønsted acidity sufficiently strong to protonate this basic probe molecule, as well as medium-strong Lewis acidity similar to that previously found over niobia, thus reasonably attributed to Nb^{5+} coordinatively unsaturated centers.

These features are confirmed by ammonia adsorption and thermodesorption experiments, allowing to calculate the amount of strong and weak acid sites at the gas/solid interface. Furthermore, 2-phenylethylamine (PEA) adsorption experiments performed at the liquid-solid interface show the higher acidity of the sample which is richer in niobium and possesses also mesoporosity. In all cases it is confirmed that the increased amount of niobia results in an increase of the concentration of surface acid sites, although the additional sites are weaker than those present in the lower-Nb-content sample.

Catalytic experiments, realized both in the Temperature Programmed Reaction mode, and in steady state conditions, reveal medium-high catalytic activity of the ternary oxides in the gas-phase acid-catalyzed conversion of ethanol to ethylene, starting from around 500 K, with a minimal or no formation of diethylether also at low temperature and ethanol

conversion. Traces of diethylether form at higher contact times suggesting that it is a secondary product formed by addition of ethanol to ethylene. However, the two catalysts also show parallel activity in ethanol dehydrogenation to acetaldehyde, which is only weakly affected by the presence of oxygen in the gas phase. The sample richer in niobium is more active, as expected indeed. Some catalyst deactivation is found, which is more significant at low temperature and for the sample with less niobium. This can be associated to the partial hindering of active sites by oligomeric carbon species over this catalyst, where adsorption experiments shows that part of active sites are sterically hindered being accessible to ammonia but unaccessible to PEA.

IR spectra confirm the data of catalytic experiments, showing the formation of strongly adsorbed alkoxide species, that decompose to ethylene above 523 K. Overall, these catalysts appear very promising for the production of bioethylene from bioethanol with a minimal coproduction of diethylether.

References.

[1] G. Busca, A. Gervasini, Advan. Catal., C. Song ed., vol. 67 (2020) 1-90.

[2] G. Busca, Micropor. Mesopor. Mat., 254 (2017) 3-16.

[3] G. Busca, Chem. Rev., 107(2007) 5366-5410

[4] G. Busca, Phys. Chem. Chem. Phys., 1, 723-736 (1999)

[5] F. Cavani, G. Girotti, G. Terzoni, Appl. Catal. A Gen., 97 (1993) 177-196.

[6] V.N. Ipatieff, R.E. Schaad, Ind. Eng. Chem. 30 (1938) 596-599.

[7] I. Nowak, M. Ziolek, Chem. Rev., 99 (1999) 3603–3624.

[8] G. Busca, G. Ramis, V. Lorenzelli, P.F. Rossi, A. La Ginestra, P. Patrono, Langmuir, 5 (1989) 911-916

[9] M.J. Campos Molina, M. López Granados, A. Gervasini. P. Carniti, Catal. Today, 254 (2015) 90-98.

[10] P.A. Burke, E.I. Ko, 129 (1991) 38-46.

[11] J.L. Vieira, G. Paul, G.D. Iga, N.M. Cabral, J.M.C. Bueno, C. Bisio, J.M.R. Gallo, Appl. Cat. A, Gen. 617 (2021) 118099.

[12] Q. Liu, H. Liu, D.-M. Gao, Chem. Eng. J. 430 (2022) 132756

[13] N.J. Clayden, G. Accardo, P. Mazzei, A. Piccolo, P. Pernice, A. Vergara, C. Ferone, A. Aronne, J. Mater. Chem. A, 3 (2015) 15986–15995.

[14] A. Gervasini, S. Campisi, P. Carniti, M. Fantauzzi, C. Imparato, N.J. Clayden, A. Aronne, A. Rossi, Appl. Catal. A, 579 (2019) 9–17.

[15] A. Aronne, M. Di Serio, R. Vitiello, N.J. Clayden, L. Minieri, C. Imparato, A. Piccolo, P. Pernice, P. Carniti, A. Gervasini, J. Phys. Chem. C, 121 (2017) 17378–17389.

[16] A. Gervasini, P. Carniti, F. Bossola, C. Imparato, P. Pernice, N.J. Clayden, A. Aronne, Mol. Catal., 458 (2018) 280–286.

[17] N.J. Clayden, C. Imparato, R. Avolio, G. Ferraro, M.E. Errico, A. Vergara, G. Busca, A. Gervasini, A. Aronne, B. Silvestri, Green Chem., 22 (2020) 7140-7151

[18] S. Ross, J.P. Olivier, On Physical Adsorption, Wiley and Sons, New York, (1964).

[19] E. Finocchio, C. Cristiani, G. Dotelli, P. Gallo Stampino, L. Zampori, Vibr. Spectrosc. 71 (2014), 47-56.

[20] K. Hadjiivanov, Advan Catal., F.C. Jentoft ed., 57 (2014) 99-318.

[21] T. Armaroli, G. Busca, C. Carlini, M. Giuttari, A. M. Raspolli Galletti, G. Sbrana, J. Mol. Catal., 151, 233-243 (2000)

[22] H.Gomez Bernal, A. M. Raspolli Galletti, G.Garbarino, G.Busca, E.Finocchio, Applied Catalysis A: General, 502 (2015) 388-398.

[23] G. Busca, Catal. Today 41 (1998) 191-206

[24] G. Busca, Progr. Mater. Sci. 104 (2019) 215-249.

[25] G. Busca, Phys. Chem. Chem. Phys., 1 (1999) 723-736

[26] C. Carlini, M. Giuttari, A. M. Raspolli Galletti, G. Sbrana, T. Armaroli and G. Busca, Appl. Catal., A Gen., 183, 295-302 (1999)

[27] M. Massa, A. Andersson, E. Finocchio, G. Busca, J. Catal. 307 (2013) 170–184

[28] G. Ramis, P.F. Rossi, G. Busca, V. Lorenzelli, A. La Ginestra and P. Patrono, Langmuir, 5, 917-922 (1989)

[29] E. Garrone, B. Onida, B. Bonelli, C. Busco, P. Ugliengo, J. Phys. Chem. B 110 (2006) 19087–19092.

[30] J. Liu, J. Yang, X. Cheng Zeng, S.S. Xantheas, K. Yagi, Xiao He, Nature Comm. (2021) 12:6141

[31] K. Nakajima, Y. Baba, R. Noma, M. Kitano,J.N. Kondo, S. Hayashi, M.Hara, J. Am. Chem. Soc. 133 (2011) 4224–4227

[32] V. Sanchez Escribano, G. Garbarino, E. Finocchio, G. Busca, Top. Catal 60 (2017) 1554–1564.

[33] G. Pampararo, G. Garbarino, P. Riani, M. Villa García, V. Sánchez Escribano, G. Busca, Appl. Catal. A, Gen. 602 (2020) 117710

[34] D. Fan, D.-J. Dai, Ho-S. Wu, Materials 6 (2013) 101-115

[35] A. Mohsenzadeh, A. Zamani, M.J. Taherzadeh, ChemBioEng Rev. 4 (2017) 75–91

[36] J. Lee, J. Szanyi, J.H. Kwak, Mol. Catal. 434 (2017) 39-48

[37] Ł. Kuterasinski, U. Filek, M. Zimowska, B.D. Napruszewska, M. Gackowski, P.J. Jodłowski, Mater. Res. Bull. 147 (2022) 111652

[38] T. Kito-Borsa, S.W. Cowley, ACS Division of Fuel Chemistry, Preprints, 49 (2004) 856-859.

[39] M. Sakuth, T. Mensing, J. Schuler, W. Heitmann, G. Strehlke, D. Mayer, Ethers, Aliphatic. In Ullmann's Encyclopedia of Industrial Chemistry; Wiley-VCH Verlag GmbH & Co. KGaA: Weinheim, Germany, 2010.

[40] T. K. Phung, G. Busca, Chem. Eng. J. 272 (2015) 560-567.

[41] G. Garbarino, R. Prasath Parameswari Vijayakumar, P. Riani, E. Finocchio, G. Busca, Appl. Catal. B Environ. 236 (2018) 490-500.

[42] H. Xia, ACS Omega 2020, 5, 9707−9713